Final Progress Report of

UGC Major Research Project

"Synthesis and Characterization of New Rare-Earth Oxoborate for Dosimetric Use"

[41-951/2012(SR)]

Submitted to

MRP Division

University Grant Commission

Bahadur Shah Zafar Marg, New Delhi-110002

By

Prof. M. Srinivas

Department of Physics

Faculty of Science

The Maharaja Sayajirao University of Baroda,

Vadodara - 390002, Gujarat, INDIA

2015

Chapter 1 Introduction

The chemistry of oxoborates directed towards a large type of new polymorphs similar to β-AB_4O_7 (A = Mn, Ni, Cu, Zn, Ca, Hg), the rare-earth meta-oxoborates ∝-$RE(BO_2)_3$ (RE = La, Ce), and a new non-centrosymmetric alteration of bismuth triborate δ-BiB_3O_6. Further on, we could expand the number of extant compositions by the high-pressure compounds $RE_3B_5O_{12}$ and $Pr_4B_{10}O_{21}$ where RE = Tm–Lu. The oxoborates of $RE_4B_6O_{15}$ (RE = Dy, Ho), ∝-$RE_2B_4O_9$ (RE = Sm–Ho), and the newly found HP–NiB_2O_4 showed the structural feature of edge-sharing BO_4-tetrahedra. The latter one describes the first borate, in which each tetrahedron gives a common edge with a neighboring tetrahedron.

The study of the High-pressure and high-temperature synthesis of oxoborates on the phase formation and crystal chemistry of the alkaline earth tetraborates ∝- CaB_4O_7 ($P2_1/n$), SrB_4O_7 ($Pmn2_1$), and BaB_4O_7 ($P2_1/c$) had done by many researchers. Under ambient pressure, the following barium borates were structurally well-characterized: ∝-BaB_4O_7 ($P2_1/c$), ∝-BaB_2O_4 (R3c, low-temperature form), β-BaB_2O_4 (R3, high-temperature form), and $Ba_5(BO_3)_2(B_2O_5)$ ($P2_12_12_1$). Other compositions are discussed well in the literature, although structurally unspecified: $Ba_3B_2O_6$, $Ba_2B_{10}O_{17}$, $Ba_2B_2O_5$, and$Ba_4B_2O_7$. ∝-BaB_4O_7 is an excellent material, exhibiting thermally stimulated luminescence with two glow peaks at 110 and 150^OC. Similar compounds previously find attractive applications, e.g. as phosphors used in thermoluminescence dosimetry.

Related to different borate structures, there is a close correlation between β-BaB_4O_7 with the acentric high-pressure phases β-MB_4O_7 (M = Ca, Hg, Sn), and the isotypic ambient-pressure phases MB_4O_7 (M = Sr, Pb, Eu).The current study in synthesis and characterization of novel inorganic borates has centered on their exceptional physical properties, which present them attractive for various practical applications like optical compounds, for instance, substances for a second harmonic generation or host matters for fluorescence. The rare-earth borates were manufactured starting from boron oxide B_2O_3 and the rare-earth oxides Ln_2O_3 whereby compound composition was seen for the molar ratios 1:1, 1:3, and 3:1 as shown below:

$B_2O_3 + Ln_2O_3 \rightarrow 2\ LnBO_3$ ---------- (1)

$B_2O_3 + 3\ Ln_2O_3 \rightarrow 2\ Ln_3BO_6$---------- (2)

$3\ B_2O_3 + Ln_2O_3 \rightarrow 2\ LnB_3O_6$---------- (3)

The rare-earth ortho-borates LnBO3 show polymorphism which is directed to a large number of studies concerning their crystallographic structures and chemical properties. It has been identified that rare-earth borates of the composition ''Ln_3BO_6'' crystallize in three different monoclinic structures as Ln varies from La to Lu.

$Gd_{17}(BO_3)_4(B_2O_5)_2O_{16}$, determined through powder X-ray diffraction data, were discovered to have an excess borate. Although the Rietveld refinements followed in fairly residual values, a couple of possibilities remained. L*n*B_3O_6 metaborates were obtained with L*n* = Y, La, Ce, Pr, Nd by Canneri, with L*n* = Pr to Tb (except Pm) by Tananaev et al., and with L*n* = La to Tb by Bambauer et al. Latterly, a new structure refinement on monoclinic $Pr(BO_2)_3$ was conducted by Sieke et al.

The compounds were reported to crystallize in four distinct space groups, i.e., $P2_1/c$ for Ln=La to Nd and C_2/m, C_2, or Cm for Ln=Pm to Yb. The combination of these compounds was only confirmed by phase analysis and was estimated to be the various rare-earth cation-rich phase in the system Ln_2O_3–B_2O_3. All these oxoborates are distinguished by high structural flexibility originated in the linkage of planar/nonplanar BO_3-groups and BO_4-tetrahedra, which can happen as isolated or condensed significant building blocks.

Examining for new compounds in the system Ln_2O_3–B_2O_3, we noticed that it is possible to obtain the new compositions $Ln_4B_6O_{15}$ (Ln=Dy, Ho) and α-$Ln_2B_4O_9$ (Ln=Eu, Gd, Tb, Dy) under extreme high-pressure and temperature conditions:

$$3B_2O_3 + 2Ln_2O_3 \xrightarrow{HP/HT} Ln_4B_6O_{15} \qquad (4)$$

$$2B_2O_3 + Ln_2O_3 \xrightarrow{HP/HT} \alpha - Ln_2B_4O_9 \qquad (5)$$

In contrast to all nearly 500 structurally characterized oxoborates, wherein the linkage of BO_3- and BO_4-units occurs exclusively via corners, it can be pointed out that these oxoborates are the first examples exhibiting edge sharing BO_4-tetrahedra next to corner-sharing BO_4-tetrahedra.The optical properties of borate crystals appear to be related

to their molecular structure. These crystals are constructed from a basic structure unit: $(BO_3)^{3-}$ anionic groups.

Originally, lithium oxoborates are practiced in Surface Acoustic Wave (SAW) devices of electric circuits. Such devices transform acoustic waves in an electrical signal and vice versa making use of the piezoelectric effect of specific materials. The significant substances used in this area are quartz, lithium niobate, lithium tantalate, lanthanum gallium silicate, and lithium tetraborate is confirmed to be a moderately logical option. Furthermore, lithium borates are understood to be used in sensors like pressure sensors and pyroelectric sensors. Owing to their nonlinear optical properties this material gets used as an ultraviolet frequency converter in lasers.

The utilization of radiation to a thermoluminescence phosphor triggers the appearance of mobile holes and electrons in the crystal structure of the substance. There is a connection between the number of engaged traps and radiation applied. The system can be described by the hypothesis that at least two shortcomings exist in the structure of a thermoluminescent material. In radiation, pairs of electrons and holes are produced. After the first excitation, one of the shortcomings captures the electron and the other imprisons a hole. These imperfections maintain different metastable trapping states and energies associated with the energy bands they are in. After the irradiation, heating of the samples delivers the electrons to the conduction band by which the electron may recombine with the trapped holes which results in the emission of photons. At this stage, the hole traps are named the “luminescent” or “recombination center”.

Chapter 2 Experimental Methods

The term combustion synthesis came from the material synthesis through the reactions method which is defined as the mercurial oxidation of the oxidants employing fuel that produces a tremendous amount of heat. In a different word, it is a method where the sequence of exothermic chemical reactions leads between a fuel and an oxidant that generate heat and the conversion of chemical varieties. Due to its adaptable nature, combustion synthesis has been employed in the synthesis of a diversity of inorganic materials such as oxides, ceramics, perovskites, metals, and semiconductor composites. In modern times, the combustion method had been associated with different scientific subjects related to material research such as materials sciences, chemistry, and physics. This method gets enormous attention in various researcher areas due to its outcome as a nanomaterial.

The combustion process is carried out through two basic modes: (i) Propagation mode; in this mode, the combustion reaction starts locally by ignition and then reaches the whole phosphor with a self-sustained propagation of the combustion flow. (ii) Volume reaction mode; in this mode, the entire phosphor is uniformly heated to the ignition temperature and the combustion reaction occurs simultaneously in all parts of the phosphor. It is also called a thermal explosion.

Out of these two-mode of combustion, the volume reaction model is most suitable for weakly exothermic combustion reactions in which preheating of the materials was required before ignition. Most of the inclusive research has been conducted by propagation mode; therefore the significant root of combustion synthesis is organized on this propagation mode. In the combustion synthesis method, the propagation of a combustion flow takes place via reaction media i.e. fuel and oxidants used for the agitation. As an outgrowth, the peculiarities of the combustion method and the synthesized phosphor are profoundly dependent on the structure and properties of the reaction media.

Experimental Method:

Rare earth doped Dysprosium Oxoborate ($Dy_2B_4O_9$) was synthesizing by combustion synthesis method and solid state reaction method. The starting materials to prepare $Dy_2B_4O_9$ are Analytical Reagent grade Dysprosium Oxide (Dy_2O_3, Purity 99.9%)

and di-boron tri-dioxide (B_2O_3, Purity 99%), were sodium peroxide use as a flux. Starting material was mix through mortar and pastel by crush thoroughly half hour, then put this mixture in aluminum crucible for combustion at $1200^{O}C$ for two hour then naturally cooled it at room temperature.

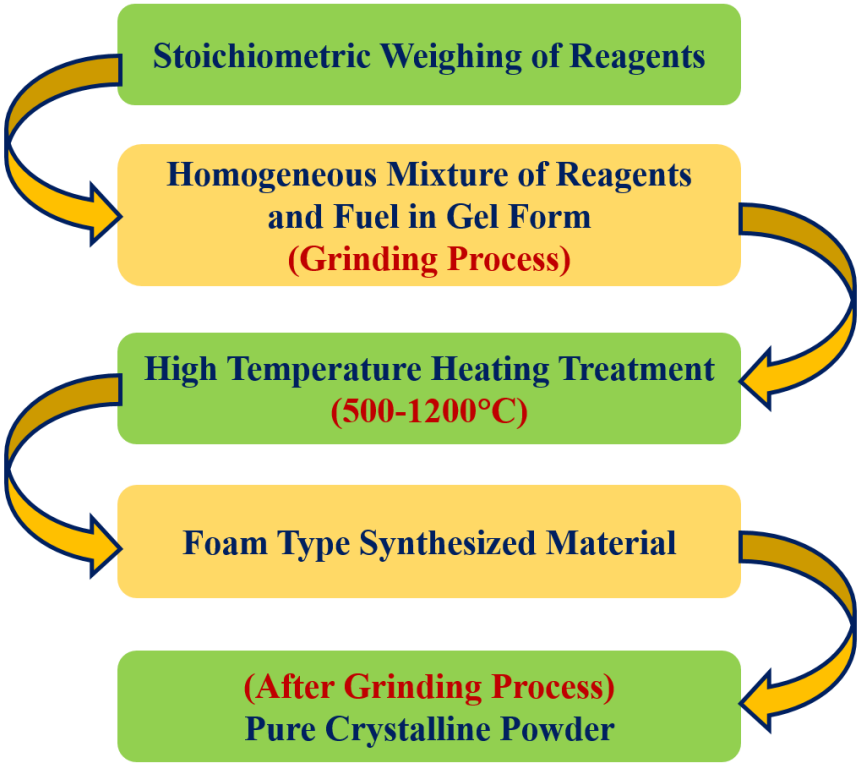

Figure2.1 Steps for conventional solid state reaction route.

According to the nature of the reaction media, the combustion process can be divided into two categories, namely homogeneous combustion, and heterogeneous combustion. In the homogeneous combustion process, both heat production, and heat transfer are constant, and the chemical reaction is homogeneous. In the heterogeneous combustion process, heat generation is discrete and heat transfer is heterogeneous. Numerous control parameters are adapted to manage the combustion method to synthesis desired materials in their several applications. The calculation of control parameters like nature of flame, temperature variation, nature of the atmosphere, chemical constitutions of precursor, fuel-oxidant ratio and generated gases, etc., should be organized accurately. Combustion synthesis is an engaging method for synthesis nano-materials for quality

applications such as catalysts, luminescent phosphors, nanomaterials for solid oxide fuel cells, materials for solar cells, and environmental remediation.

Characterizations:

X-Ray Diffraction (XRD)

The powder X-Ray Diffraction (XRD) pattern involves intense peaks exhibited due to the constructive interference of a monochromatic x-ray beam scattered at distinct angles from various sets of lattice planes developed in the material. Peak intensities in the XRD pattern can determine the allocation of atoms within the lattice and the spacing between the planes. The XRD pattern is the nature of the periodic order of atoms in a material. The peak intensities of the XRD pattern depend on certain factors such as structure parameter, incident intensity, slit width, operating voltage, and electric current of the X-ray source.

FTIR

FTIR spectroscopy is the efficacious characterization method for the identification of existing functional groups in the materials for both organic and inorganic. The mid-infrared spectrum with a range of 4000 cm^{-1} – 400 cm^{-1} used in Infrared spectroscopy for the classification of the fundamental rotational and vibrational mode in material structure. The fingerprint region of the IR spectrum 400 cm^{-1} to 1500 $cm^{-1}$is the most important region to identify the fundamental groups present in the material. FTIR is used to identify unknown components present inside the mixture. FTIR spectroscopy is the study of the function of the molecules during the interaction of matter with light radiation. The IR waves combine with the polar molecules of the chemical bonds. In the absence of polarity or dipole moment in the molecule, IR interaction is insensitive as a result the molecules do not produce any IR spectrum.

Photoluminescence

Photoluminescence (PL) is the phenomenon of the emission of light from the material under optical excitation through UV, visible or infrared radiation. The absorption of UV, visible or infrared region of the spectrum begins the excitation of the valence electrons. Classification of luminescence phenomenon is constantly based on the electronic configuration of the material in which provides the excited state and the emission path to the electron. Photoluminescence is dividing into two types, fluorescence, and phosphorescence. Usually, in the fluorescence process, the emission of light happens in the

time of the order of a nanosecond. The phosphorescence process of the emission of light takes place in the period of the order of microsecond to hours or even days. The photoluminescence (PL) phenomenon is also classified based on the large-scale inorganic materials that usually exhibiting phosphorescence, as well as the smaller organic dye molecules and inorganic nanomaterials.

Thermoluminescence

Thermoluminescence (TL) is the phenomenon of emission of light transpiring from materials having a wide energy gap like insulators and semiconductors entered the absorption of energy from the radiation source. The absorption of radiation energy results in the excitation of unconfined electrons and holes. The trapping of these electrons and holes transpires at defects or trapping states in the energy gap of the material. The emission of radiation happens when the material is fired consequently after extraction of the excitation. The thermic energy use to release the electrons from defects which then recombine with the holes. If the radiative emission occurs due to the recombination process of an electron, the emission is termed thermoluminescence (TL). The basic definition of the TL phenomenon given in the subsequent statement is similar to the Thermally Stimulated Luminescence (TSL) phenomenon: "*TL necessitates the perturbation of the system from a state of thermodynamic stability, through the absorption of external energy in a metastable state, then it is accompanied by the thermally stimulated relaxation of the system back to its equilibrium condition*".

In the specific case of TL, the perturbation process is the consumption of energy from ionizing radiation, and then the thermally stimulated relaxation (TSR) back to equilibrium, which is accompanied by controlling radiative emission of luminescence from the system through the transitions of the charges back to the ground state. The TL intensity of the emitted luminescence is associated with the rate at which the system returns to equilibrium.

Chapter 3Results and Discussion

X-Ray Diffraction

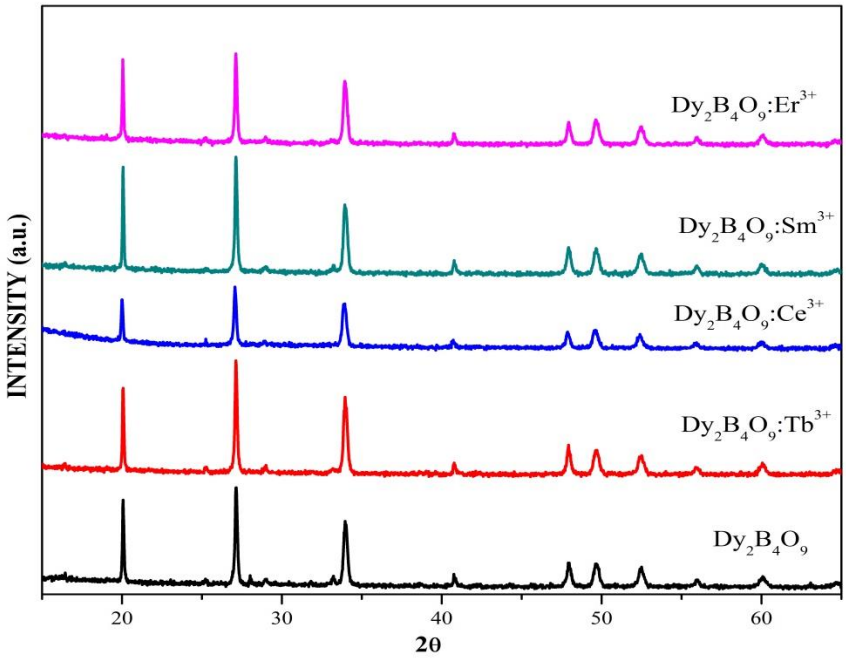

Figure 3.1 XRD spectra of $Dy_2B_4O_9$ with different doped.

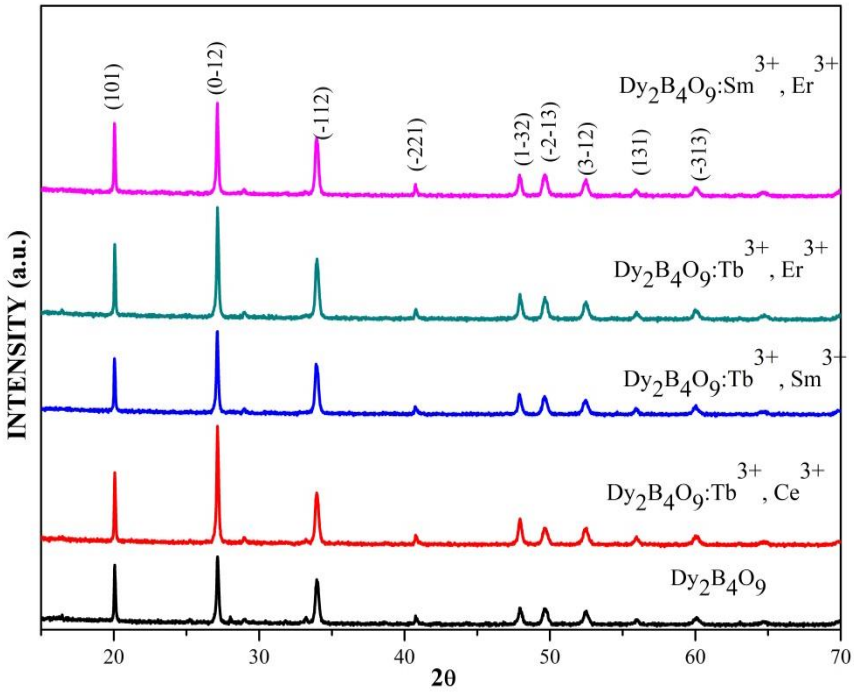

Figure 3.2XRD spectra of double-doped $Dy_2B_4O_9$.

Figure 3.1 and 3.2 shows X-ray diffraction spectra of undoped, single doped and double rare earth doped $Dy_2B_4O_9$. From study of X-Ray Diffraction, we find that all the samples of undoped, single doped and double-doped $Dy_2B_4O_9$ have triclinic structure with space group $P\bar{1}$ (no. 2). The crystalline size of all the samples are average 40nm which find using Scherer's formula $D_{crystallite} = \frac{k\lambda}{BCos\theta}$, where B is full width half maxima, k is a shape factor of the particle (it is 1 if the spherical shape), λ and θ are the wavelength and the incident angle of the X-rays, respectively. The effective XRD peak broadening can cause by lattice strain and small crystallite size; these two effects have to be distinguished. This can calculate by plotting β cosθ versus 4sinθ in the relation $\beta_{hkl} * \cos\theta_{hkl} = (k\lambda/D) + 4\sin\theta_{hkl}$ (Williamson–Hall plot). The shift in the XRD patterns reflected in the Williamson–Hall plot, which attributed due to the highly strained and distorted environment in the undoped and double-doped $Dy_2B_4O_9$.

Table 3.1 Strain and Crystallite size of singly doped $Dy_2B_4O_9$

Compound	**$Dy_2B_4O_9$**	**$Dy_2B_4O_9$:Tb**	**$Dy_2B_4O_9$:Ce**	**$Dy_2B_4O_9$:Sm**	**$Dy_2B_4O_9$:Er**
Strain	3.86×10^{-3}	7.2×10^{-3}	-1.0×10^{-2}	2.7×10^{-3}	-6.4×10^{-4}
Crystallite Size (Scherer's Formula)	28.2nm	29.66nm	18.38nm	25.79nm	20.45nm

Table 3.2 Crystallite size of double doped $Dy_2B_4O_9$

Compound	**$Dy_2B_4O_9$:Tb, Sm**	**$Dy_2B_4O_9$:Tb, Er**	**$Dy_2B_4O_9$:Tb, Ce**	**$Dy_2B_4O_9$:Sm, Er**
Crystallite Size (Scherer's Formula)	39.66nm	35.38nm	42.79nm	37.45nm

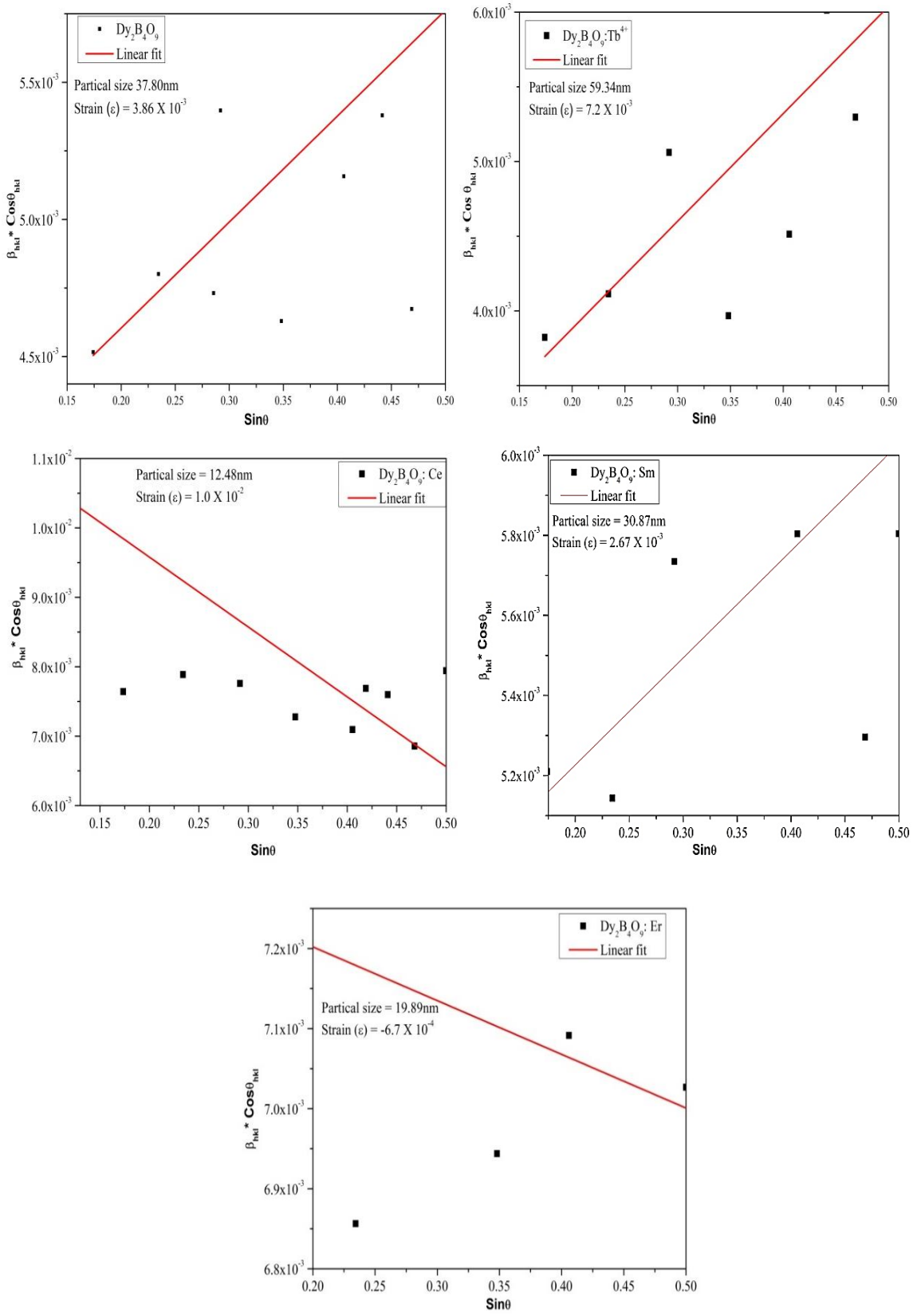

Figure 3.3 Williamson- Hall plot for $Dy_2B_4O_9$ with different doped

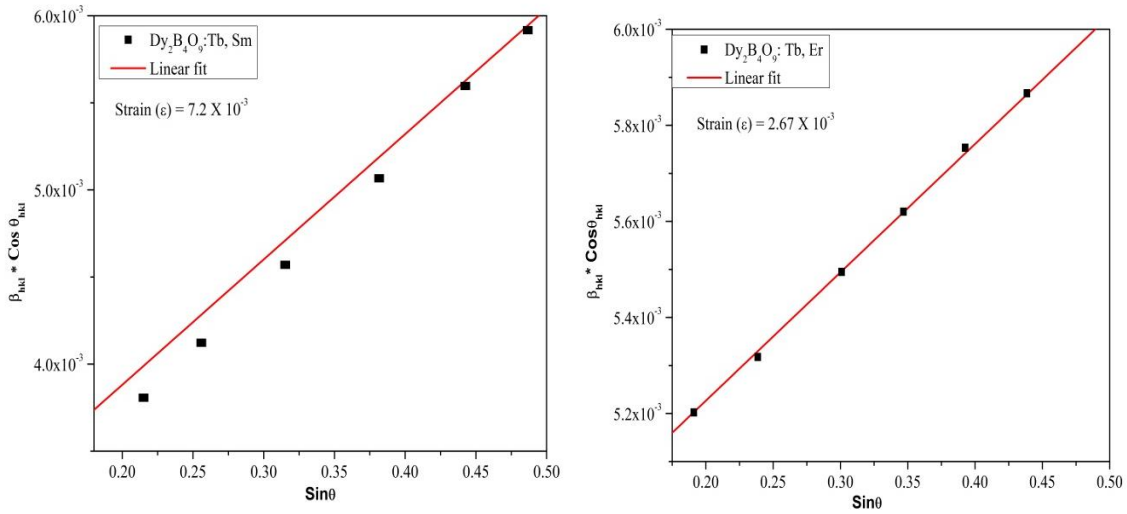

Figure 3.4 Williamson- Hall plot of double doped $Dy_2B_4O_9$.

Fourier Transform Infrared Spectroscopy (FTIR):

Fig. 3.5 and 3.6 exhibit FTIR spectra of undoped, single doped, and double doped $Dy_2B_4O_9$. Usually, separated planar BO_3-groups with trigonal symmetry show four fundamental modes of vibration, symmetric stretching (ν_1 = 900cm^{-1}–1000 cm^{-1}), the out of plane bending (ν_2 = 700 cm^{-1}–780 cm^{-1}), the antisymmetric stretching (ν_3 = 1100 cm^{-1}–1300 cm^{-1}), and the in-plane bending (ν_4 = 590cm^{-1}– 680 cm^{-1}). The ν_3 and ν_4 are doubly degenerated and ν_1 is ordinarily inactive in the infrared.

Due to the crystalline conditions, ν_1 may become active and the degeneracy of a plane (ν_3) and in-plane (ν_4) vibration can be removed. The transmittance peaks between 790 cm^{-1} and 1200 cm^{-1} show the tetrahedral borate group BO_4 as in YBO_3, $GdBO_3$, or $TaBO_4$. The absorption peak of the triangular BO_3-group appears between 1450 cm^{-1} and 1200 cm^{-1} and for less than 790 cm^{-1}. Due to the sequence of one BO_3- and three crystallographic independent BO_4-units in the solid-state, the detailed assignment of the vibrations is difficult.

The material mainly consists of crystalline parts of $Dy_2B_4O_9$. From wavenumber 4000 cm^{-1} to 2800 cm^{-1} there no absorption bands were observed due to OH. In IR spectra, the strong and broad absorption peak in the region 1170 cm^{-1} - 1400 cm^{-1} corresponds to the asymmetric stretching vibrations (ν_3) of the BO_3- groups. Also, the strong and usually sharp absorptions derived from the out-of-plane bending (ν_2) of the trigonal ion occur in the range 730 cm^{-1} – 790 cm^{-1}. The absorptions between 600 cm^{-1}to 650 cm^{-1} are attributed

to the in-plane bending (ν_4) of the BO_3-groups. According to the crystalline environment, the vibrations in the range 920 cm^{-1} – 940 cm^{-1} can classify as symmetric stretching vibrations. The filmed IR spectrum confirms the presence of BO_3-groups in the crystal structure of $Dy_2B_4O_9$.

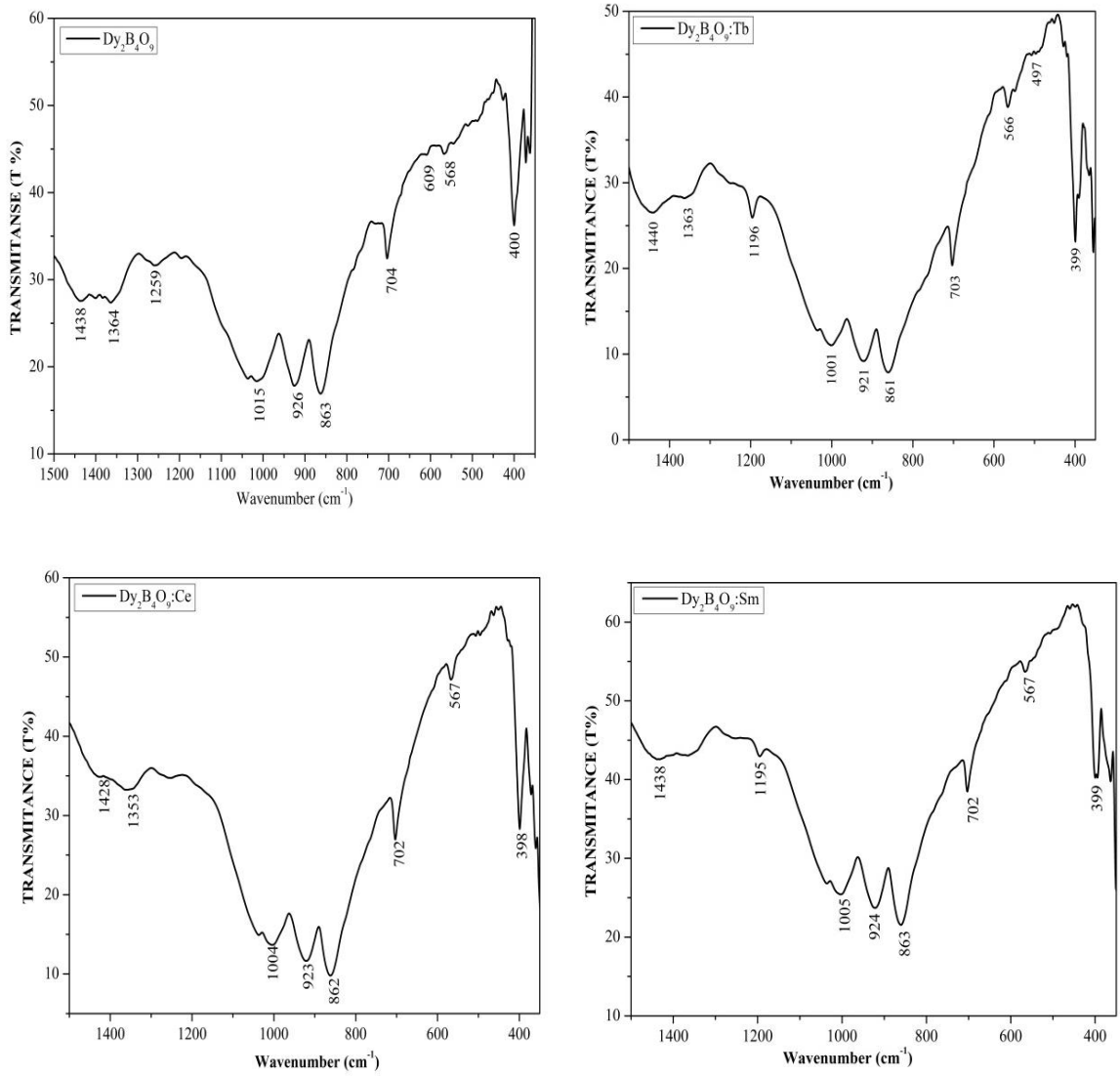

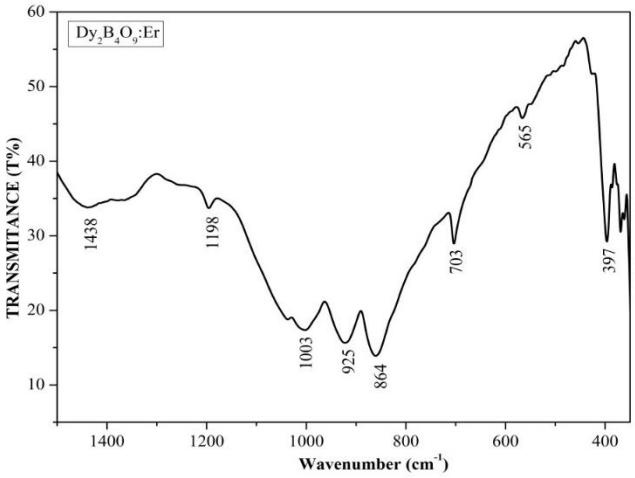

Figure 3.5 FTIR spectra of $Dy_2B_4O_9$ with different single doped.

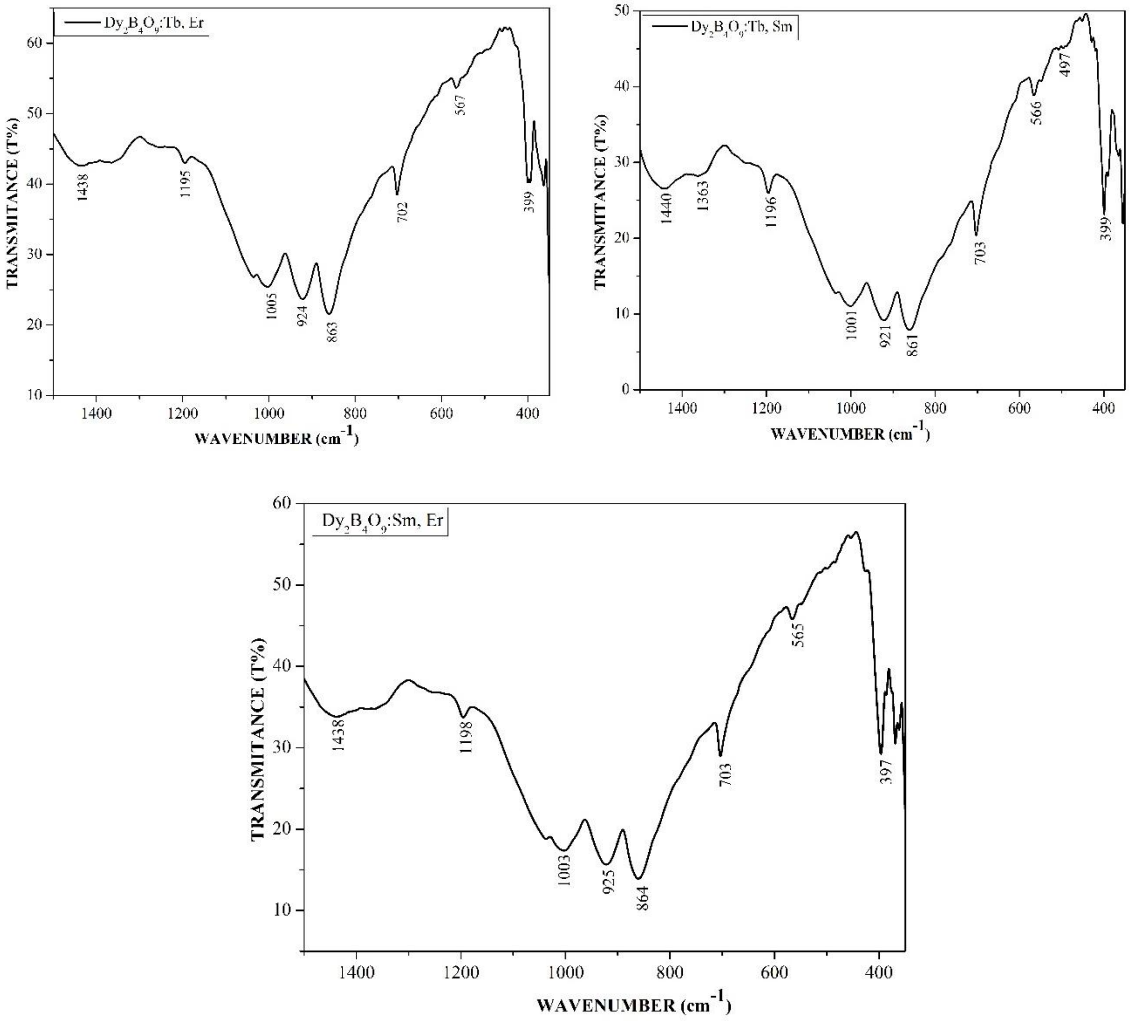

Figure 3.6 FTIR spectra of double-doped $Dy_2B_4O_9$.

Photoluminescence

In the photoluminescence, the mechanism of excitation and emission methods have been classically expressed by the Polish physicist Prof. Alexander Jablonski by the Jablonski energy level diagram as shown in Figure 3.7. At room temperature, the atoms or molecules can usually occupy the deepest vibrational energy level of the ground state to accomplish its stability. After the absorption of energy, atoms or molecules are promoted to the excited states. As exhibited in Figure 3.7, the absorption of radiation energy by the atom or molecules of the phosphor can promote the ground state electrons to either in the first excited state S_1 or second excited state S_2. There are distinct energy levels associated with the excitation and emission process.

In the Jablonski diagram, S_0 is the singlet ground state, while S_1 and S_2 are the first and second excited singlet states which are systematized in a stack formation as horizontal lines. The lowest energy level in each state expresses the electronic energy levels, and the other higher-order lines represent the different vibrational energy levels.

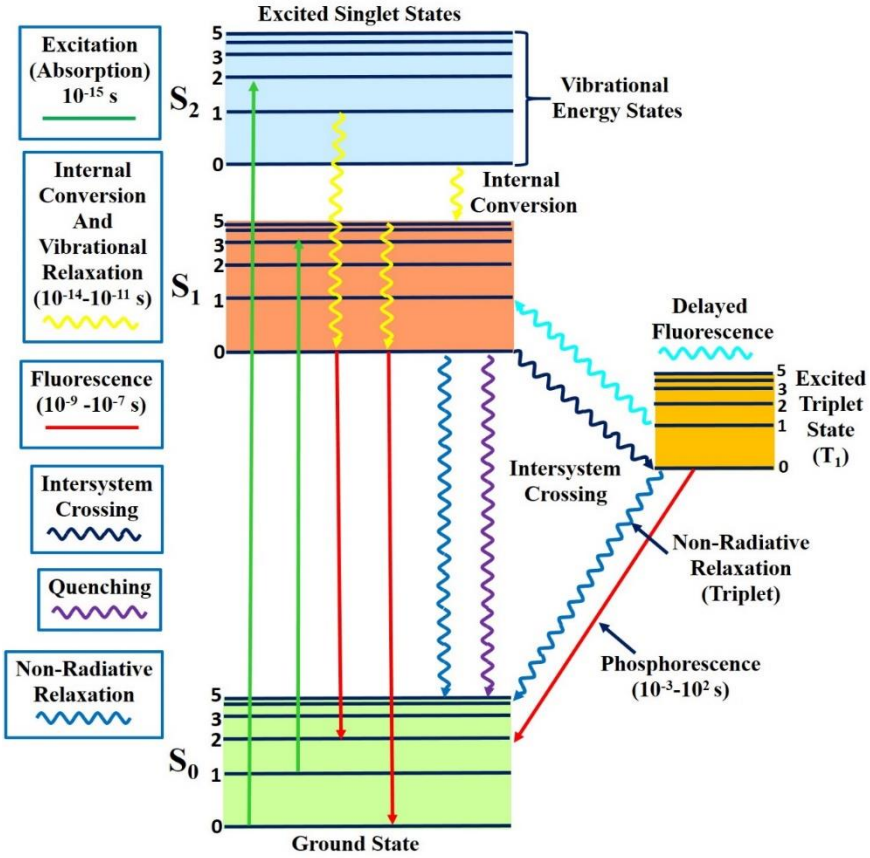

Figure 3.7 Jablonski energy level diagram for the photoluminescence mechanism.

The light emission from the phosphors can happen through three important manners, which can take place at different timescales. In the first process, after the absorption of radiation energy, the excitation of the molecule can occur in femtoseconds. In a second manner, the vibrational nonradiative recreation of excited electrons to the lowest energy level can take place in picoseconds. In the third process, the emission of a longer wavelength photon through the return of the excited molecule to the ground state can occur after a long period of the order of nanoseconds.

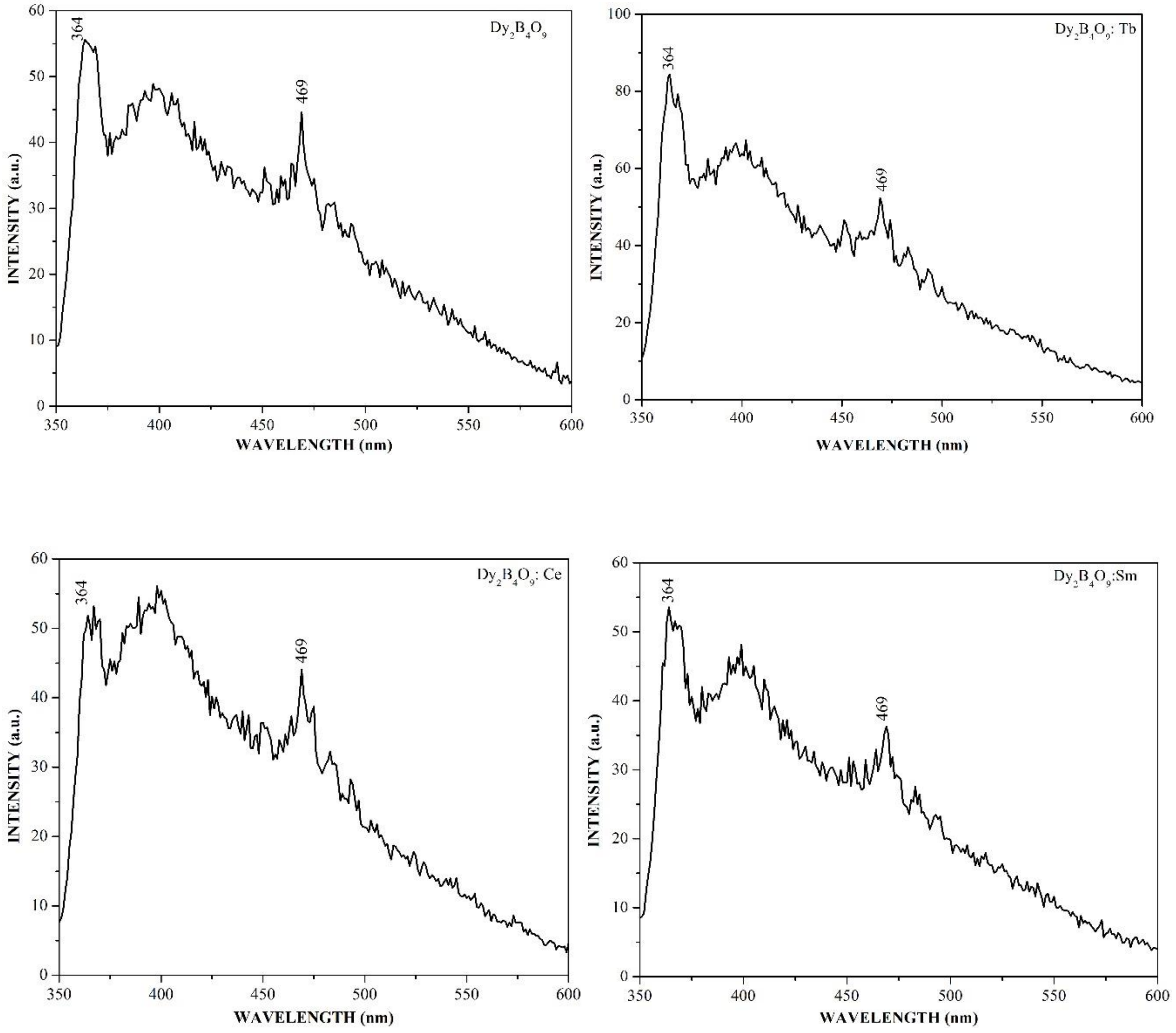

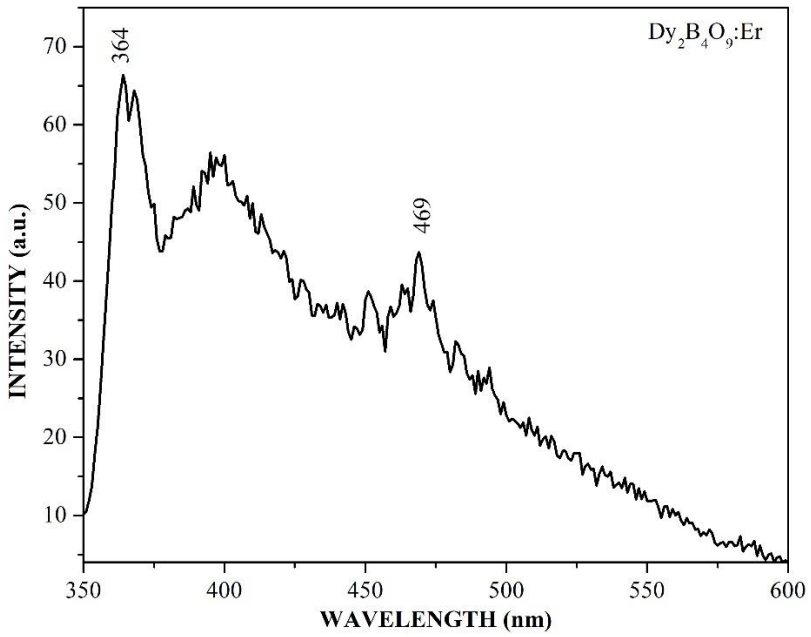

Figure3.8 Photoluminescence spectra of rare earth doped $Dy_2B_4O_9$.

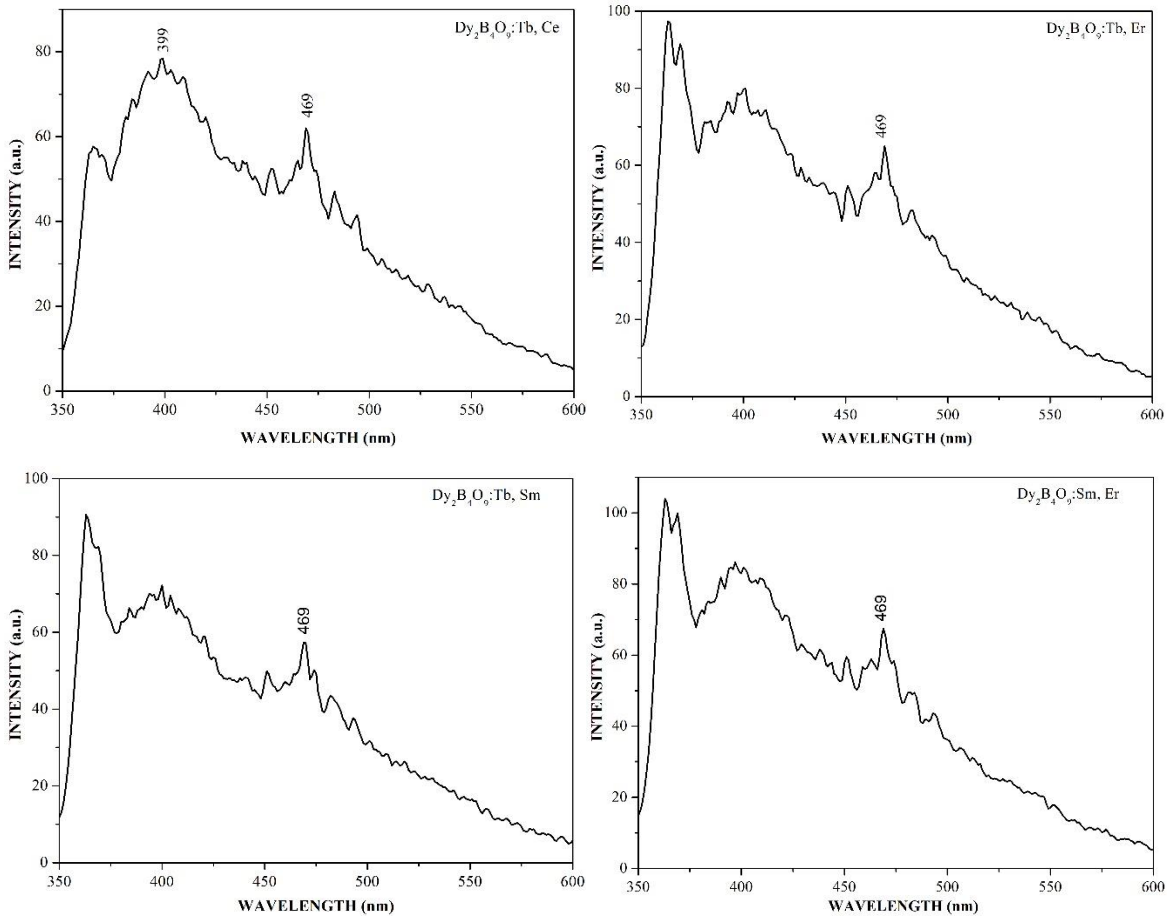

Figure3.9 Photoluminescence spectra of double rare earth doped $Dy_2B_4O_9$.

Figures 3.8 and 3.9 present room temperature photoluminescence spectra of different rare-earth-doped $Dy_2B_4O_9$ excited with 254nm wavelength. PL is a non-destructive technique generally used to study the photo-physical and photochemical properties in photo-assisted reactions. It is almost associated with surface stoichiometry and the characteristics of surface states, which can be changed by the heating process. The PL spectra exhibit emissions at 367nm and 469nm wavelength. The emission line at 367nm wavelength is in the UV region whereas the emission line at 469nm is in the blue region. The transition involved in the blue region at 469nm arises due to the transition of $_4I^{15/2}$ to $_6H^{15/2}$ of Dy^{3+}.

Thermoluminescence

Mechanism

The fundamental technical theory of pure crystalline luminescence materials normally established and is mainly dependent on the ‘‘collective electron” model of Bloch which has been practiced by many researchers. The approved energy levels exhibited for electrons in phosphors constituted the band structure of energy levels separated by an energy gap. In the energy levels, the valance electron of atoms is responsible for the luminescence process. In an ideal lattice structure the lattice defects, impurity, and other disorders create discrete energy levels. In another type of phosphors, impurity ions or larger complex factors can take part as luminescence emission centers at the discrete energy levels. This phosphor provides energy levels to trap electrons just below the conduction band of the semiconducting or insulating phosphors. The proposed energy levels in the forbidden gap may be discrete and depending on the nature of the defect and type of host lattice. This kind of electron trap inside the forbidden gap has been responsible for the phenomenon of phosphorescence and thermoluminescence.

Through the excitation, electrons emitted from the valence band progressing throughout the crystal may be 'trapped' inside a hole due to the Colombian field attraction of an unoccupied anion site. The minimum energy required to emit an electron from the trap center is much smaller than the energy required for releasing a valence electron. Therefore the anion vacancy allows a metastable energy state between the valence band and the conduction band. A similar kind of energy level occurs due to cation vacancies

where the missing cation creates a deficiency of positive charge, as a result, the energy required to release an electron from the neighboring anion can decrease. The vacancies in the crystal structure are responsible for the generation of confined energy levels inside the forbidden gap. The composition of the localized energy levels inside the forbidden gap is determined by the decrease in the energy needed to release the electron from the discrete energy level. The energy level occurs due to the anion vacancies have energy more than Fermi energy as a consequence before-mentioned energy levels are located above the Fermi energy level and are empty of electrons which can potential electron traps. Similarly, the energy level arises due to the cation vacancies have an energy less than that of the Fermi energy, as a result, such energy levels situated below the Fermi energy level and are full of electrons which can potentially hole trap. A similar kind of condition has been taking place under the incorporation of substitutional or interstitial impurity ions formed within the crystal lattice. The introductory energy band diagram for an insulator or semiconductor containing electron and hole trapping levels is shown in Figure 3.10.

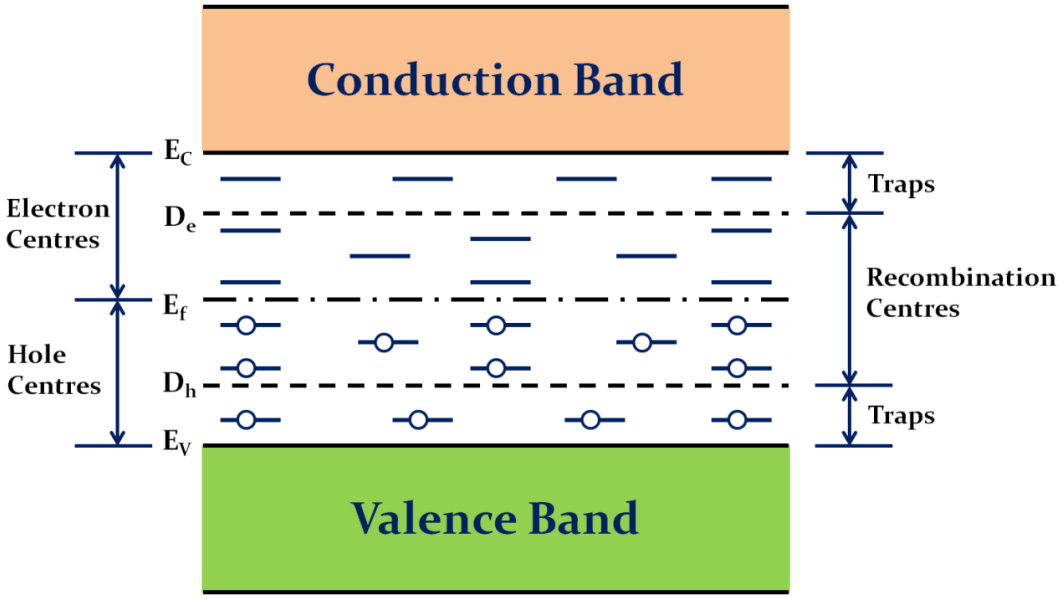

Figure 3.10 Energy levels diagram of an insulator and semiconductor at absolute zero temperature.

The type of TL mechanism in wide energy gap material is founded on band theory. According to this theory, the ionizing radiation energy is employed which creates free electrons, holes, and defects in the material. The following methods take place in the TL mechanism:

- ***Trapping through luminescent centers (LCs):*** Diverse types of contaminant ions can form electron-hole traps in the energy gap with a free charge carrier. The radiation of a photon (radiative recombination) can happen if the opposite charge can transfer the empty trap and recombines with the earlier trapped charge. The ejection of photons largely depends on the properties of the impurity ion.
- ***Trapping by non-radiative centers:*** The free charge carriers (cation/anion) can form the confined states, not only with luminescence centers but also with other different ions. The basic essential nature of band states cannot remain the same, it could be often changed. When the charge carrier of the opposing sign arrives to fill the trap, it recombines with the earlier trapped charge, but the energy released dissipates without emission of photons (non-radiative recombination).
- ***Mutual recombination:*** Some of the free charge carriers of different signs can recombine in the matrix without trapping by luminescence centers and non-radiative centers.
- *Available charges can be recombined with defects of opposite charges at trapping centers via both radiative and non-radiative transition.*
- ***Thermal activation eviction of electrons and holes from traps:*** The confined electrons and holes create a bound state with a trapping center at the different energy states. The binding energy of these trapping centers defines the lifetime or the disintegration possibility of the bound state. The disintegration credibility increases with increasing temperature.
- ***Redistribution of charge carriers between traps and luminescence centers due to thermal excitation into the conduction band and valence band:*** The charge carriers can exhibit due to thermic activation from filled traps in the arrangement can be retrapped by all other blank traps, i.e. both luminescence centers and non-radiative centers.

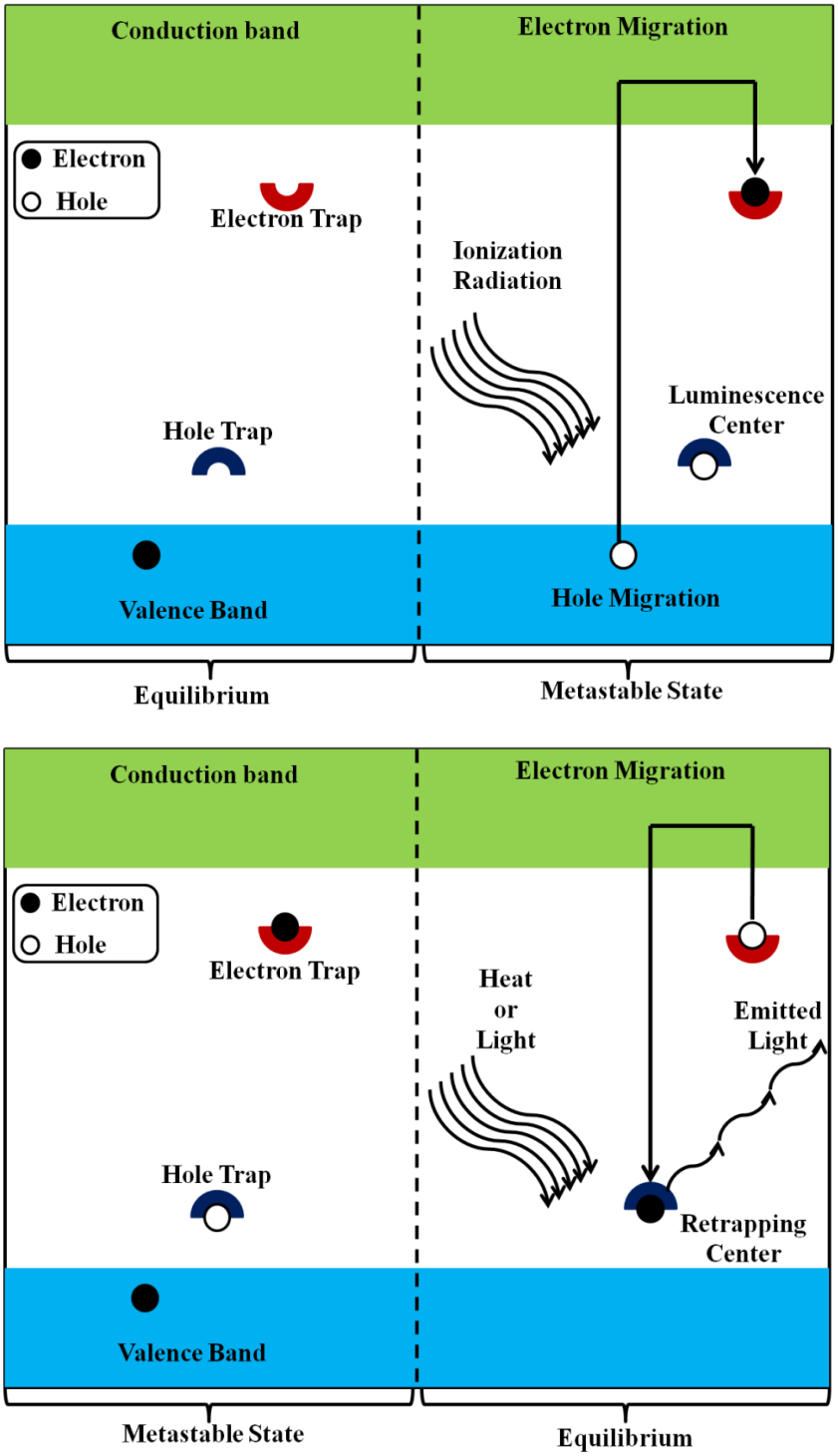

Figure 3.11 (a) Energy-level diagram of the energy storage stage for TL processes; (b) Energy-level diagram of the energy release stage for TL processes.

Figure 3.11(a) shows a mechanism of the storage process of the irradiation energy by excitation and the electron-hole pair creation. When the phosphor is irradiated by some ionization radiation, the electrons can be excited to the conduction band from the valance band as a resulting hole forms in the valence band. These excited electrons cannot remain stable in the conduction band and find a tendency to accumulate into an electron trap as well as the holes also occupy their related trap. In this method, the hole traps are termed the luminescence centers. Figure 3.11(b) shows the thermoluminescence process in which trapped electrons release their stored energy by emission of a photon when the temperature increases. In this process, the trapped electron is released through the conduction band and re-trapped with the hole trap named recombination center.

Instrumentation

The electronic functional block diagram of the TL reader conjugated with the PC system and TL reader software is shown in Figure 3.12. PC controlled TL reader type TL1009 fabricated by Nucleonix used for TL measurements of the phosphor is shown in Figure 3.13.

The TL reader consists of the following divisions of electronic circuits and other components.

***Low Voltage Supply*:** It is a DC power supply circuit that provides a low voltage of the order of +5V @ 1A, +/- 12V @ 0.5A, +24V @ 0.5A. It produces the power required for the functionality of all the circuits. It contains an input line filter circuit, a step-down transformer with four secondary voltages, a three-terminal regulator (bridge rectifier), and filter capacitors.

***High Voltage Module*:** High voltage power supply accommodates the desire biasing voltage require to the photomultiplier tube because this tube is negatively biased to DC mode of processes in the voltage range of 0 V to - 1500V. The output of a high voltage supply is a highly maintained regulated voltage supply that forms (0 to -1500V) @ 1.0mA with less than 30mV rippled & noise (peak to peak).

***PMT bleeder circuit*:** The main work of the photomultiplier tube (PMT) is to distinguish the light photon emitted when the heating process of phosphor that incident onto it and convert the light due to TL emission into D.C. current. PMT is biased through a bleeder resistor network that runs it in low dark current mode. DC output of the PMT from the

anode is applied to the I-F converter. For the DC mode operation, the photocathode of the PMT is joining to the negative bias, and an anode is connected with virtual zero potential.

***I-F (current to frequency) converter*:** A charge balancing type of current to frequency (I-F) converter circuit is practiced in the TL reader. It has better linearity than 1% over a frequency range from 1 Hz to 100 kHz. The work of the I-F circuit is to convert anode current from the PMT to continuous pulses of frequency proportional to the current.

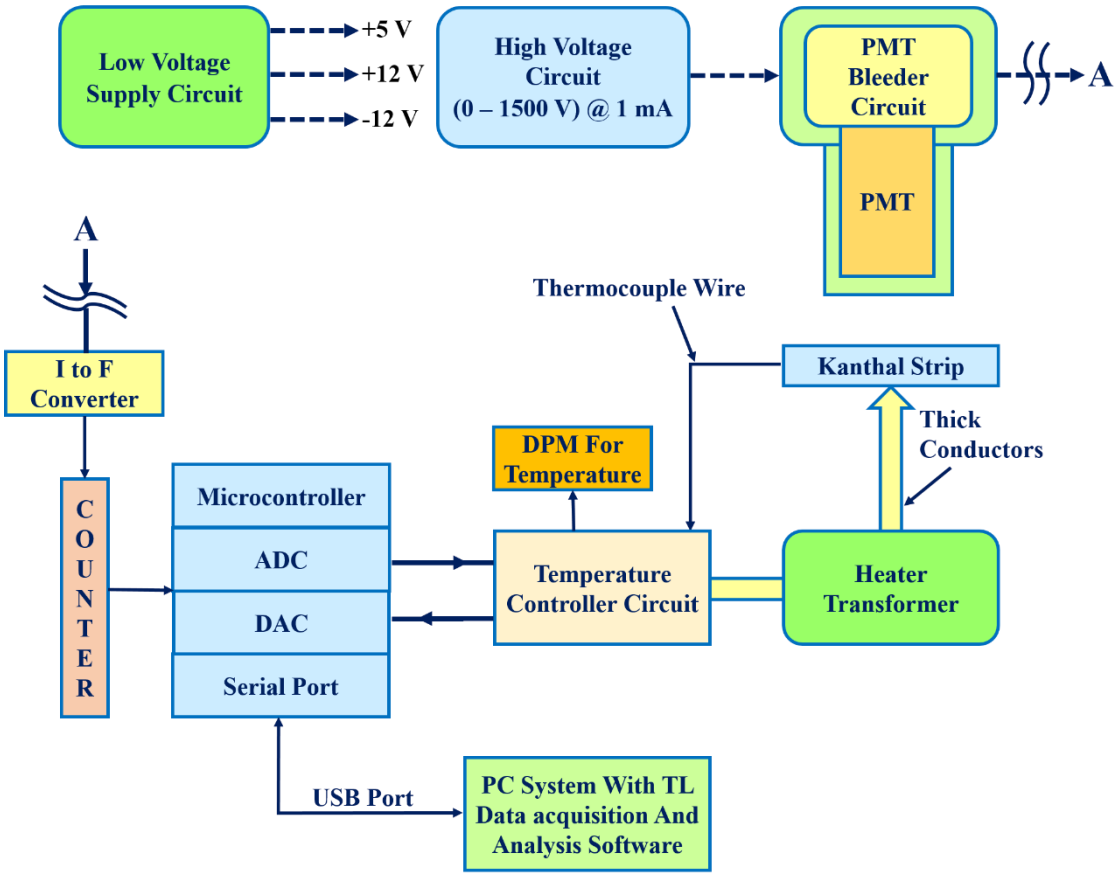

Figure3.12 Block diagram of the TL Reader.

***Microcontroller with BCD counter, ADC, DAC, serial port*:** The main work of this part of the TL instrument is the temperature calibration and interpret it in terms of actual temperature, produce several heating profiles & heating rates, command instructions from the PC, to accept TTL pulses from I to F converter which corresponds to TL intensity data and storing them in memory.

***Temperature controller*:** The temperature control system is consists of a heater transformer, heater element with the thermocouple, millivolt amplifier, display modules

(DPM). In this system, the thermocouple output of the order of millivolt collected from the kanthal strip is feed to the monolithic thermocouple amplifier and the output from this is feed to an op-amp amplifier to properly condition the signal level. This signal is further fed to digital DPM that can be calibrated to show the temperature of the kanthal strip. The signal consequently goes to ADC where the value of the signal is read by a microcontroller and interpreted in terms of temperature by a PC program. Heater strip can be programmed to heat the sample from 1°C/sec to 40°C/sec and the max set temperature allowed is 500°C for various heating profiles.

***Personal computer system* with *Data acquisition and analysis software*:** Personal computer (PC) system with TL instrument function software produces required graphical TL glow curve data procurement and analysis software. The software offers the following function: Heating profiles such as Linear, Single & Multi-plateau, Temperature Calibration, Light Stimulation Profile, Acquisition, Background spectrum / Sample data can be acquired, Background Subtraction, Export Spectrum data to Excel, Spectrum overlap, Spectrum subtraction.

.

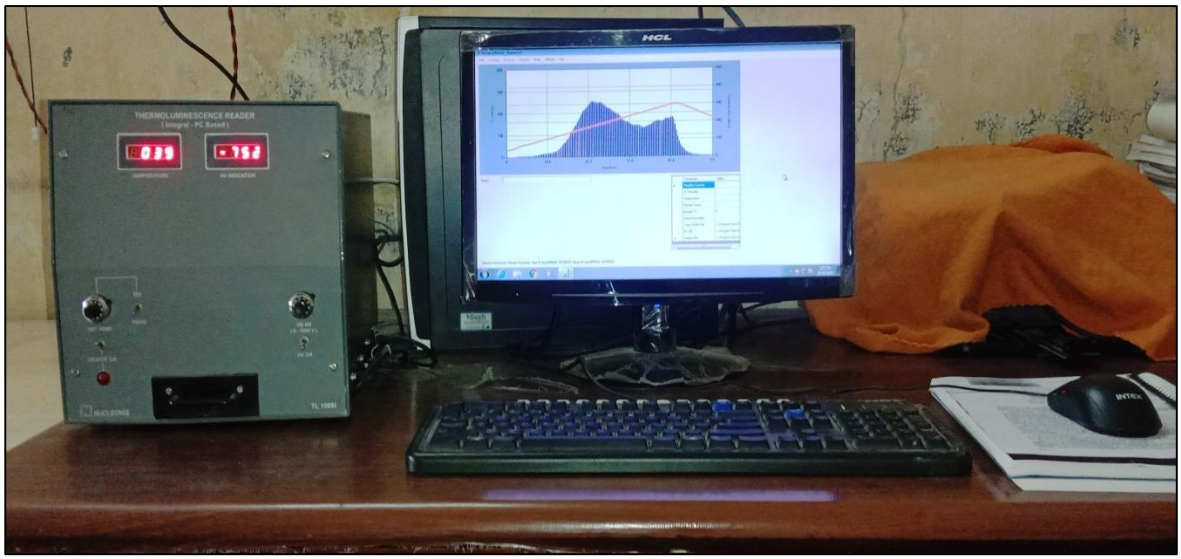

Figure3.13 PC controlled TL reader type TL1009 manufactured by Nucleonix.

Applications

The TL phenomenon has been extensively investigated by numerous researchers to know the mechanism included in thermally stimulated emission and its application. However,

due to the deep expertise of the TL mechanism, the modification and improvement in the TL instrumentation improved the researchers in diverse fields to solve their problems. Out of the large area of application, some of the applications are explained shortly. Figure 3.14 displays some significant applications of the TL phenomenon in the present world in the chart.

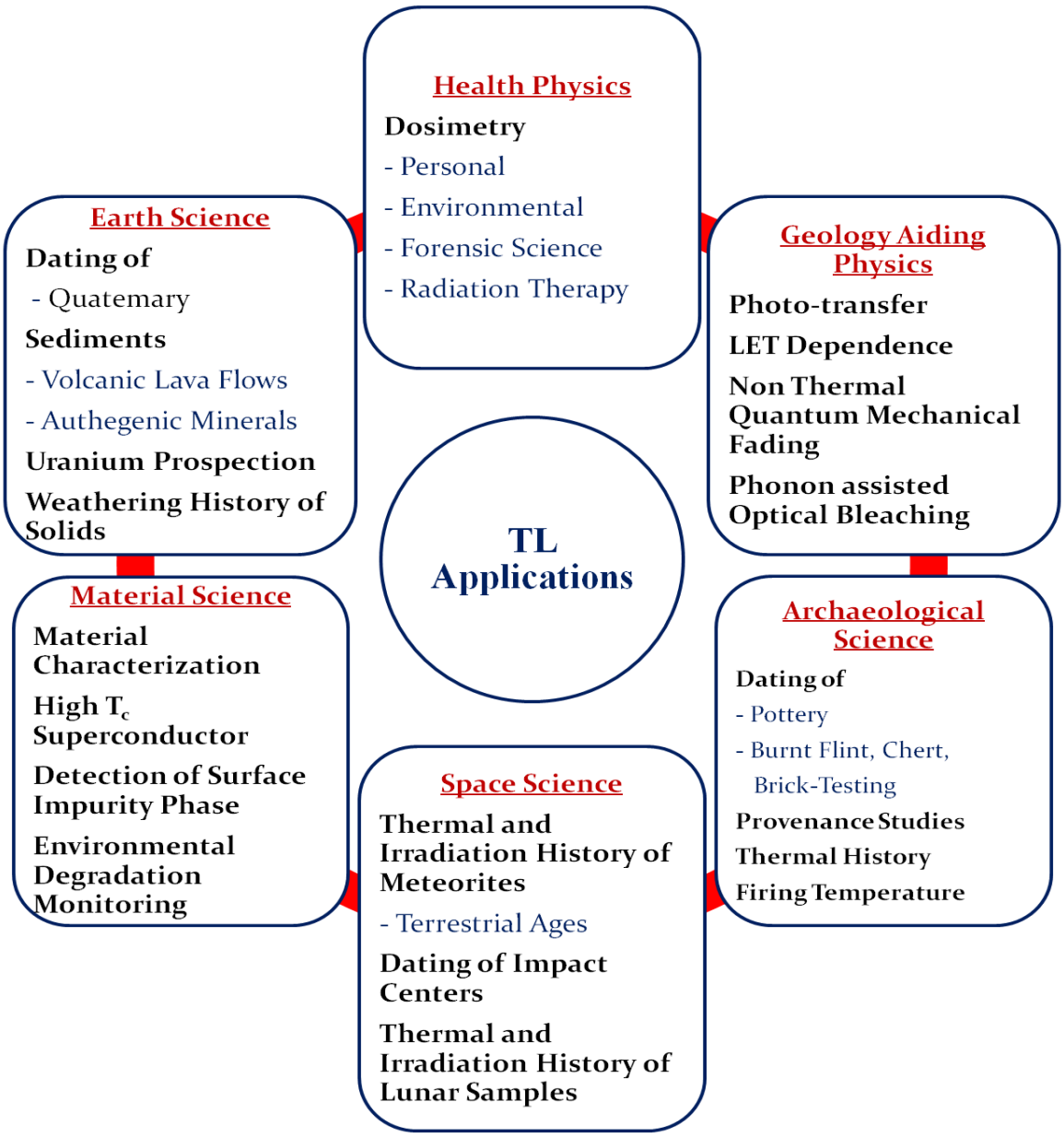

Fig. 3.14 Chart of applications of TL in different research disciplines.

TL Dosimetry (TLD)

Radiation dosimetry applications are the fundamental requirement for the computation of ionization radiations and radioisotopes, mainly in Medical Physics and Science. Ionizing radiations often occur at places, where X-rays, gamma radiation, and beta particles are mostly used for diagnosis and radiotherapy. X-rays are utilized in a security system on airports, and radiations are emitted during the experimental studies in Physics and other Science branches. High-energy electrons, heavy particles, and neutrons are used in major medical centers.

TL dosimeter is a device that is used to measures the direct or indirect ionization radiation quantities like exposure, absorbed dose or equivalent dose, or their time derivatives (rates). The selection of a phosphor for a TLD application needs well-defined data of the specific application for its users to be under consideration. TLD applications are mainly distributed into three-part that are the personal dosimetry for dose calculation of body tissue, environmental dosimetry for dose estimation in the environment, and medical dosimetry applications. The performance of a dosimeter is appraised by examining properties such as linearity, dose range, energy response, reproducibility, stability of stored information, isotropy, the effect of environment on dosimeter performance, batch inhomogeneity, and others. Some of these properties are now discussed in some detail before proceeding to a discussion of individual phosphors.

Personnel Dosimetry

In personal dosimetry, the radiation dose measurement has been performed to measure the radiation absorbed by the personnel for the duration of their repetitious occupational exposure at working place. There are several working fields like nuclear industry, workers deal with X-ray units, hospital medical physicists, radiotherapy technicians, workers in industrial radiography, high-intensity gamma irradiators, and personnel on nuclear power plants, etc. Based on observing such measures of exposure, it is known that the personnel absorbed radiation under specified safety limits, which are guided by the International Commission of Radiological Protection (ICRP) for diverse fields of application of radiation sources. The most fitting TLD used for personnel dosimetry must have the

desired characteristics such as tissue equivalent, Low fading, Accuracy (± 10% from 100 µGy to 10 Gy).

Environmental Dosimetry

In recent years, pollution due to nuclear radiation creates a critical problem in the health of living organisms. The pollution mostly produces due to gamma and UV radiation which is harmful to a human being. The environmental regulatory authorities in developed and underdeveloped countries show more awareness about environmental health. In numerous countries, environmental radiation monitoring has been done by TLD systems installed near the sources of nuclear radiation as well as the ionization radiation where it produces, such as nuclear power stations, low-level waste disposal, nuclear fuels reprocessing units, nuclear power industry, etc. The phosphor used for the environmental dosimetry does not require the tissue equivalence size. But the environment monitoring time is much longer so the material requires a long exposure. Therefore the TLD phosphor for environmental dosimetry has more stability and highly sensitive to low radiation exposure.

Medicinal Dosimetry

TLD material is broadly used in medical science for calculating suitable ionizing radiation doses given to patients during the diagnosis. For that TLD exposed throughout the treatment are recovered for examining radiation dose, which determines actual doses given to crucial internal organs during these procedures and from such data can prescribe essential additional treatments. There are many departments where clinical radiation is revealed to the humans such as x-ray exposure in mammography, dentistry, and general health screening and radiotherapy. The range of radiation dose used in radiology from 10^{-5} Gy to 10^{-2} Gy, and up to 20-60 Gy in radiotherapy. The TLD phosphors used in medical dosimetry tissue equivalency is the more important factor for the good TLD as well as the low radiation absorbance capacity of the phosphors.

All samples were firstly irradiated by Sr^{90}β-source having decay rate 5 mCi for different time intervals for the doses of 0.048 to 0.48 Gy with an accuracy of ±10%. The TL study was completed to investigate the dosimetry applications of synthesized phosphors. To achieve the purpose of application of the phosphors, TL characteristics of phosphor such as

fading effect after exposure, linearity of TL output with doses, sensitivity for the reusability of phosphor were examined through the proper layout of experiments.

$Dy_2B_4O_9$: Ce^{3+}

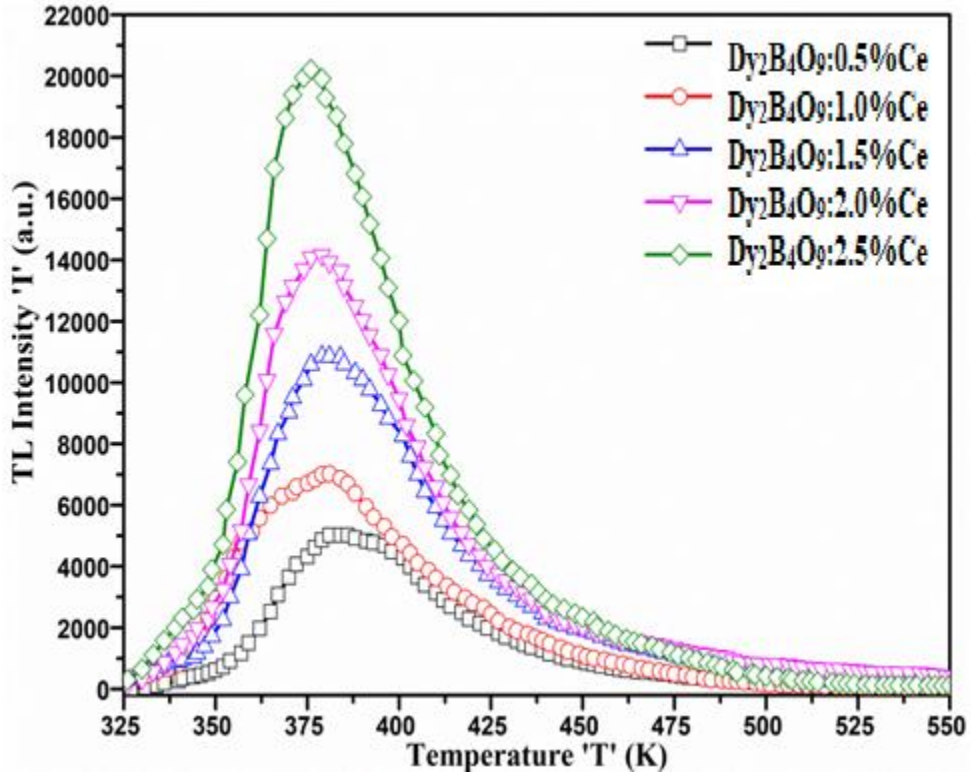

Figure 3.15 TL glow curve of $Dy_2B_4O_9$: X Ce^{3+} (X = 0.5, 1.0, 1.5, 2.0, 2.5 mol%) phosphors irradiated by β-radiation for 5 minute of 0.48 Gy dose.

Thermoluminescence (TL) characteristics of Ce3+ doped Dy2B4O9 phosphors were analyzed by examining TL output deviation based on doping concentration, the influence of irradiation time (Dose), linearity of TL intensity with amount of dose and fading effect in TL outcome with time, etc. For the study of TL properties, all the doped phosphors were irradiated by Sr90 b-source having a decay rate of 5 mCi for different time intervals of 1, 2, 3, 4, and 5 minutes. Figure 3.15 displays the TL glow curves of Ce3+ doped Dy2B4O9 phosphor irradiated by b-radiation for 5 minutes recorded for the temperature range 325 K – 550 K. All glow curves were recorded for all Ce3+ doped phosphors in powder form at the heating rate of 6 K/s the samples in fine powder form. Figure 14 shows the TL glow of Ce3+ doped Dy2B4O9 carried out after b-irradiation of phosphors by 5 mCi Sr90 b-source for different irradiation time 1 to 5 minute, i.e., 0.097 to 0.48 Gy. The TL glow curves of Ce3+ doped Dy2B4O9 phosphor exhibit a prominent

emission glow peak at 383 K temperature. The highest TL intensity is observed for the phosphor doped with 2.5 mol% Ce3+ and 5-minute radiation dose, which is for maximum concentration and maximum dose b-irradiation. The dose concentrations for different irradiation time intervals are given in Table 3.1. The dose concentration has been calculated for 10 mg samples.

Irradiation Time 't'	**Radiation Dose (D)**
30 s	0.048 ± 0.005 Gy
1 minute	0.097 ± 0.01 Gy
2 minute	0.19 ± 0.02 Gy
3 minute	0.29 ± 0.03 Gy
4 minute	0.39 ± 0.04 Gy
5 minute	0.48 ± 0.05 Gy

Table 3.1 Radiation dose values for different irradiation time for β-radiation of Sr^{90}.

The TL glow curves are showing the same kind of nature, i.e., uniform shape and structure for the different concentrations of Ce^{3+} doping. The TL outcomes of phosphor revealed that TL intensity of the glow curves increases linearly with doping concentration. The reason for increment in the TL intensity is the concentration of trapping center arises due to occupancy of Ce^{3+} increases within the host structure. TL study of Ce^{3+} of $Dy_2B_4O_9$ phosphor showed that doping of Ce^{3+} enhances the TL property of the host. Because undoped $Dy_2B_4O_9$ phosphor showed poor TL properties due to the perfect crystal structure or may be due to low intrinsic defect, which cannot be useful for measure the absorbed dose. Doping of Ce^{3+} can raise the trap centers in the energy gap due to the incorporation of Ce^{3+} ions in the host structure at the Dy^{2+} site, which steadily increases with doping concentration also identified in photoluminescence analysis, and resulting in the high TL performance.

Figure 15 shows the TL glow curve fitting of 2.5 mol% Ce^{3+} doped $Dy_2B_4O_9$ phosphor by GCD fitting method for general order kinetics. GCD fitting of the glow curve follows Kitis et al. equation of general order kinetics given by equation

$$I(T) = I_M b^{b-1} exp\left(\frac{E_a}{k_B T} \cdot \frac{T - T_M}{T_M}\right)$$
$$\times \left[(b-1)\frac{T^2}{T_M^2} \cdot \left(1 - \frac{2k_B T}{E_a}\right) exp\left(\frac{E_a}{k_B T} \cdot \frac{T - T_M}{T_M}\right) + 1\right.$$
$$\left. + -1)\frac{2k_B T_M}{E_a}\right]^{-\frac{b}{b-1}} \ldots\ldots\ldots\ldots\ldots\ldots\ldots\ldots\ldots\ldots\ldots\ldots\ldots\ldots\ldots\ldots\ldots\ldots\ldots\ldots\ldots\ldots (1)$$

TL glow curve has been fitted for fine value of figure of merit (FOM) 0.017% calculated by equation

$$FOM = \frac{\sum_p |I_{Exp} - I_{Th}|}{\sum_p |I_{Th}|} \ldots\ldots\ldots\ldots\ldots\ldots\ldots\ldots\ldots\ldots\ldots\ldots\ldots\ldots\ldots\ldots\ldots\ldots\ldots\ldots\ldots\ldots\ldots\ldots (2)$$

using experimental and theoretically fitted TL glow curve. The GCD fitting of the glow curve exhibited that the glow curve comprises five peaks at different temperatures with different peak intensities as stated in Table 3.1. This fine fitting signifies that there could be five electron traps produced in the energy gap at various energy depths. The quantity of electron traps is raised at a different energy level in the forbidden bend due to dose increment and increase Ce3+ doping concentration. This results in the decline of widening of TL glow curve with increasing concentration and intensity increase quickly. The interpretation of the fitted curve exhibited that the peak-I, Peak-II, peak-III, peak-IV, and peak-V have an order of kinetic "b" values 1.8, 1.8, 2.0, 1.9, and 2.1 respectively that reflects the second-order kinetics.

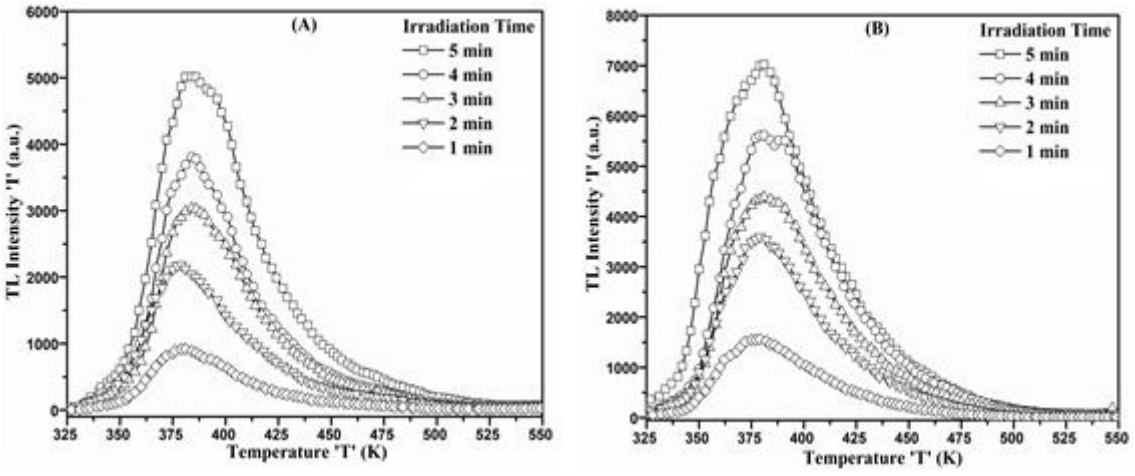

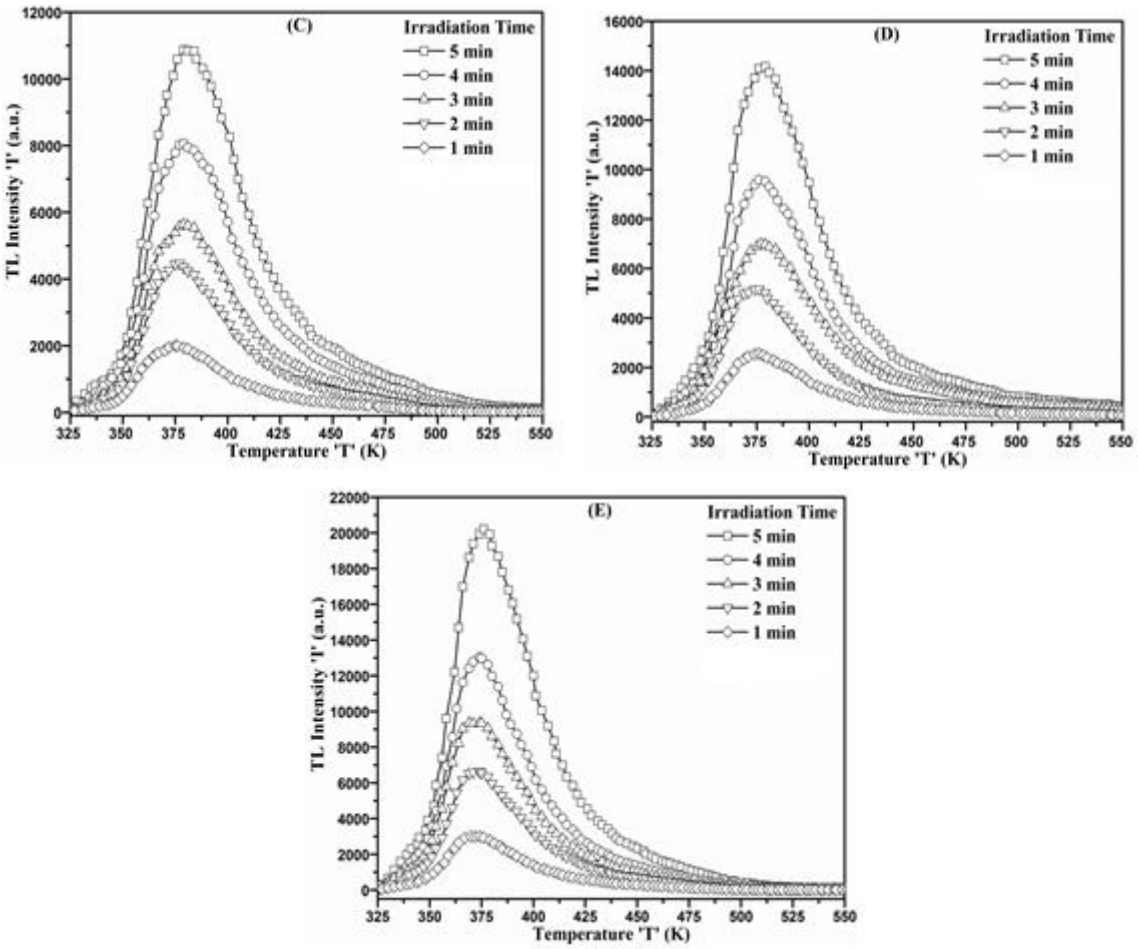

Figure 3.15 TL glow curves for various time of β-irradiation: (A) $Dy_2B_4O_9$: 0.5mol% Ce^{3+}; (B) $Dy_2B_4O_9$: 1.0 mol% Ce^{3+}; (C) $Dy_2B_4O_9$: 1.5mol% Ce^{3+}; (D) $Dy_2B_4O_9$: 2.0mol% Ce^{3+}; (E) $Dy_2B_4O_9$: 2.5 mol% Ce^{3+}.

The activation energy requires for capturing electrons from the trap center is provided to the phosphor by heating the sample. The computed values of activation energy 'Ea' and the frequency factor 's' for various trap centers in 2.5 mol% Ce^{3+} doped $Dy_2B_4O_9$ phosphors were calculated through the GCD method and are compiled in Table 3.2. Frequency factors 's' of each deconvoluted peaks were calculated from the equationfor second order kinetics.

$$s = \frac{\beta E_a}{k_B T_M^2 \left(1 + \frac{2kT_M}{E_a}\right)} exp\left(\frac{E_a}{k_B T_M}\right) \dots\dots\dots\dots\dots\dots\dots\dots\dots\dots\dots\dots\dots\dots (3)$$

The activation energy 'E_a' of different peaks of 2.5 mol% Ce^{3+} doped $Dy_2B_4O_9$phosphor are ranging from 2.41 to 0.57 eV. Frequency factor 's' are ranging 10^{11} to $10^{13}s^{-1}$ for different peaks.

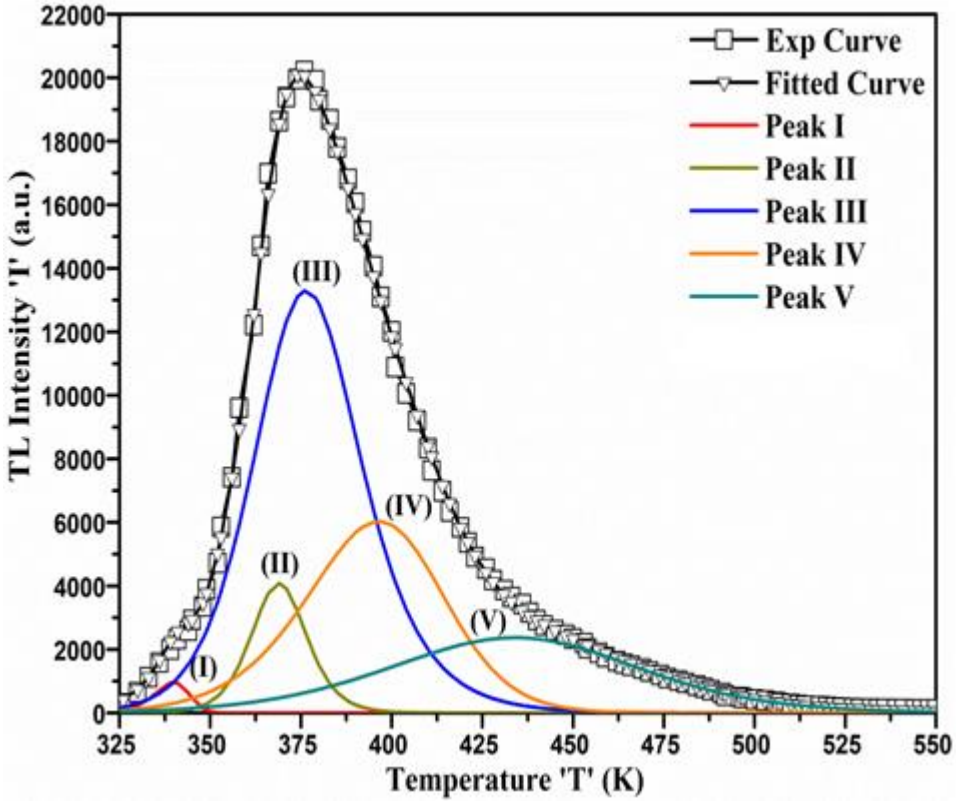

Figure 3.16GCD fitting of TL glow curve of 2.5 mol% Ce^{3+} doped $Dy_2B_4O_9$ irradiated by β- radiation for 5 minute of 0.48 Gy dose.

TL glow curve parameter also measured by Chen's peak shape method (PSM) for second-order kinetics. The activation energies included in the glow curve formation of 2.5 mol% Ce^{3+} doped $Dy_2B_4O_9$ phosphors are determined by Chen's peak shape method (PSM). The formula for second-order kinetics of PSM is given by the following equations (4), (5), and (6).

$$E_\tau = \frac{1.72k_BT_M^2}{\tau} - 1.874(2kT_M) \ldots\ldots\ldots\ldots\ldots\ldots\ldots\ldots\ldots\ldots\ldots\ldots\ldots\ldots (4)$$

$$E_\delta = \frac{1.487k_BT_M^2}{\delta} \ldots\ldots\ldots\ldots\ldots\ldots\ldots\ldots\ldots\ldots\ldots\ldots\ldots\ldots\ldots\ldots\ldots\ldots\ldots\ldots (5)$$

$$E_\omega = \frac{3.234k_BT_M^2}{\omega} - 2kT_M \ldots\ldots\ldots\ldots\ldots\ldots\ldots\ldots\ldots\ldots\ldots\ldots\ldots\ldots\ldots (6)$$

TL parameters calculated by Chen's PSM is given in Table 3.2. The calculate values of geomantic factor 'μ_g' in PSM as mentioned in Table 3.3 are approximately equivalent to the value of second order kinetics. That proposes the PSM analysis is also truthful as GCD method.

Sample		Activation Energy 'E_a' (eV)	Order Of Kinetics 'b'	FOM %	Frequency Factor 's' (s^{-1})
$Dy_2B_4O_9$: 2.5 mol% Ce^{3+}	Peak I	2.37±0.06	1.8	0.017	1.17×10^{11}
	Peak II	2.15±0.06	1.8		2.23×10^{12}
	Peak III	1.17±0.05	2.0		7.54×10^{12}
	Peak IV	0.88±0.03	1.9		3.45×10^{13}
	Peak V	0.57±0.01	2.1		8.63×10^{13}

Table 3.2 Summary of TL kinetic parameters of glow curve for sample 2.5 mol% Ce^{3+} doped $Dy_2B_4O_9$irradiated by β-radiation for 5 minute of 0.48 Gy dosecalculated by GCD method.

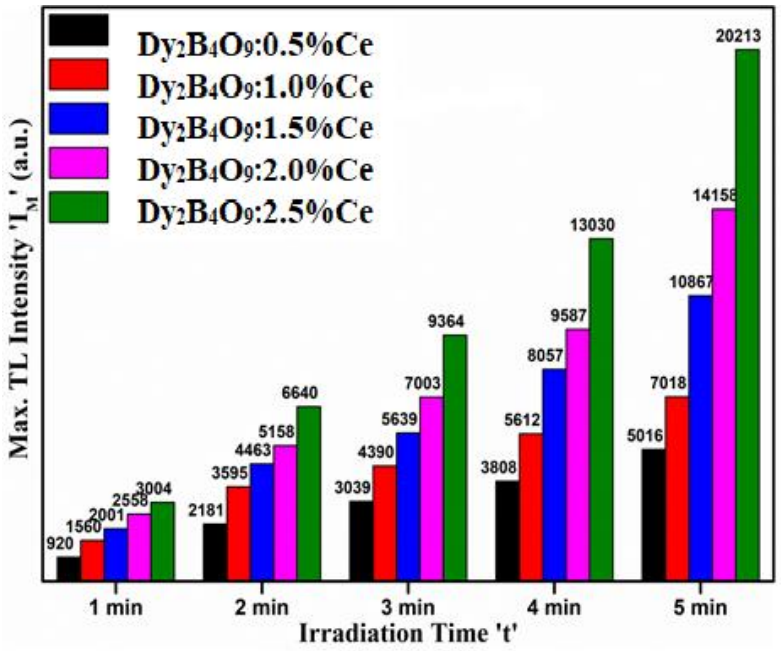

Figure 3.17 Maximum TL intensity 'I_M'vs β-irradiation time 't' graph of Ce^{3+} doped $Dy_2B_4O_9$.

Sample		I_{max}	T_{max} (K)	T_1 (K)	T_2 (K)	τ (K)	δ (K)	ω (K)	μ_g	Activation Energy		
										E_τ (eV)	E_δ (eV)	E_ω (eV)
$Dy_2B_4O_9$: 2.5 mol% Ce^{3+}	Peak I	949.3	339	333.5	345	5.5	6	11.5	0.522	2.41±0.06	2.45±0.04	2.43±0.05
	Peak II	4079.7	369	361.5	377	7.5	8	15.5	0.516	2.17±0.03	2.18±0.05	2.15±0.03
	Peak III	13295.1	376	359	394	17	18	35	0.514	1.15±0.04	1.13±0.03	1.16±0.02
	Peak IV	6028.2	395	373	418	22	23	45	0.511	0.92±0.02	0.87±0.02	0.90±0.01
	Peak V	2370.2	433	393	474	40	41	81	0.506	0.55±0.01	0.58±0.01	0.58±0.01

Table 3.3 Summary of TL kinetic parameters for 2.5 mol% Ce^{3+} doped $Dy_2B_4O_9$irradiated by β-radiation for 5 minute of 0.48 Gy dose calculated by PSM.

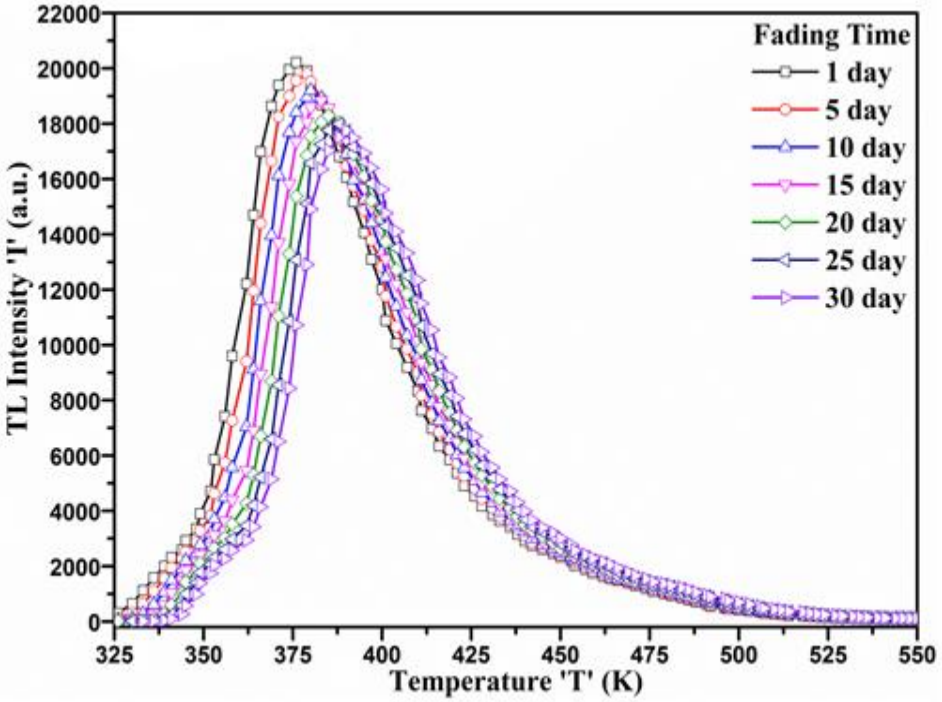

Figure 3.18 TL glow curve of $Dy_2B_4O_9$: 2.5 mol% Ce^{3+} phosphor irradiated by β-radiation for 5 minute of 0.48 Gy dose.

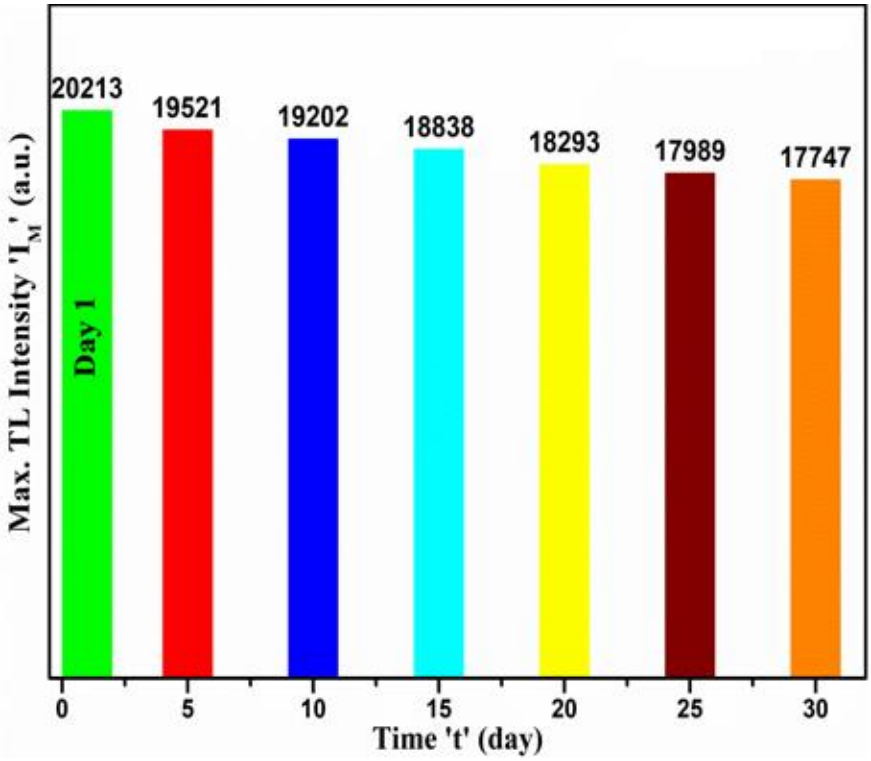

Figure 3.19 Maximum TL intensity 'I_M'vs Fading time 't' graph of $Dy_2B_4O_9$: 2.5 mol% Ce^{3+} phosphor irradiated by β-radiation for 5 minute of 0.48 Gy dose.

The phosphors utilized for dosimetry purposes have specific characteristics such as TL intensity peak of glow curve should be constant, the effect of fading in TL peak should be zero or least after radiation exposure and reusability of phosphors. Figure 3.17 exhibits the Maximum TL intensity vs b-irradiation time (t) graph of Ce^{3+} doped $Dy_2B_4O_9$ for varying concentrations of doping ion. The location of the TL glow curve of the Ce^{3+} doped $Dy_2B_4O_9$ phosphor is steady for various dose exposure and doping concentrations. TL intensity of Ce^{3+} doped $Dy_2B_4O_9$ phosphor changes linearly with radiation dose and doping concentration. The TL glow curves were obtained to analyze the fading effect of the TL glow curve at the period of five days for one month for all phosphors. The phosphors were stored in dark situations at room temperature after exposure to β-irradiation. Figure 3.18 presents the TL glow curve of $Dy_2B_4O_9$: 2.5 mol% Ce^{3+} phosphors irradiated for 5-minute b- radiation to perceived fading effect with time after exposure. The fading study of Ce^{3+} doped $Dy_2B_4O_9$ phosphor showed that the TL glow curve temperature peak shifted towards high temperature as the time transpired, but the fading of peak maximum is much low about 2 - 3% per five days. A similar kind of fading effect was seen in all phosphors with varying concentrations and doses. Figure 3.19 shows the Maximum TL intensity vs Fading time (t) graph of $Dy_2B_4O_9$: 2.5 mol% Ce^{3+} phosphors irradiated for 5-minute β- radiation.

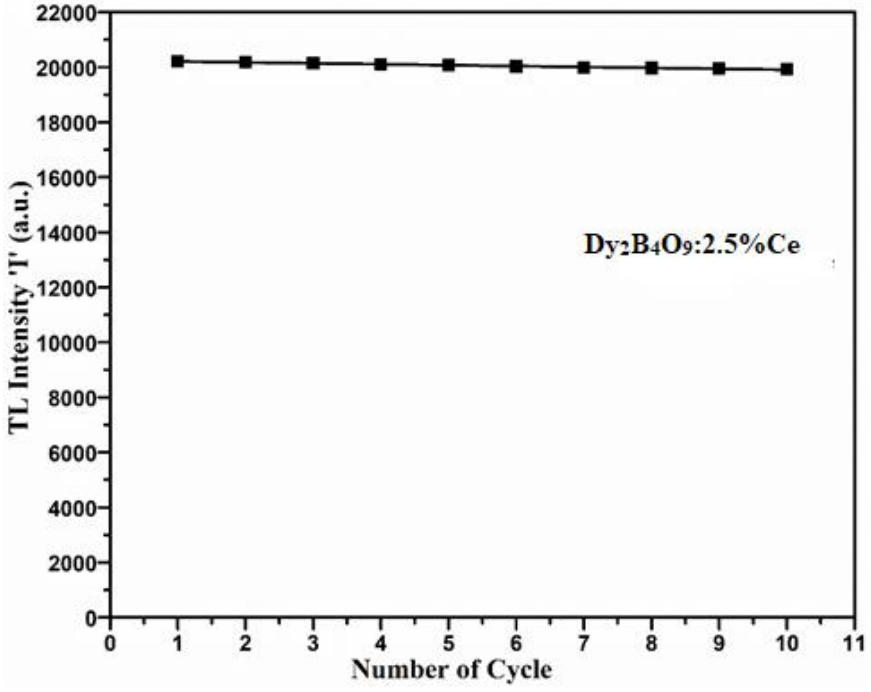

Figure 3.20TL intensity vs Number of cycles of uses for $Dy_2B_4O_9$: 2.5 mol% Ce^{3+}.

The TL glow curve obtained from Ce^{3+} doped $Dy_2B_4O_9$ was consistent after a long period of exposure to beta particles, which provides information about the charge storage capacity of the $Dy_2B_4O_9$ phosphor. The sensitivity of TL phosphor was studied by observing the TL outcome of the phosphors by exposing the same phosphor many times. That provides the notable result, where the TL intensity of the phosphor fractionally changed after repeated uses is less than 7% from first to the tenth use of phosphor as shown in Figure 3.20 for 2.5 mol% Ce^{3+} doped $Dy_2B_4O_9$ phosphors. The outcome shows the significance of TL parameters like activation energy of traps remains constant after repeated readouts. Thus, Ce^{3+} doped $Dy_2B_4O_9$ can be considered a good phosphor for TLD application.

The interpretation of glow curves showed the significance of the TL mechanism requires in glow curve formation. The activation energy, frequency factor, and order of kinetics assessed by both methods are similar and consistent. The activation energy of different peaks demonstrates that the trap is formed at distinct energy levels which order different excitation energy for de-trapping in holes. The calculated values of trapping parameters by two different methods are very similar that provides the significance of the TL outcome of Ce^{3+} doped $Dy_2B_4O_9$ phosphor.

SUMMARY OF THE PROJECT REPORT ENTITLED:

"Synthesis and Characterization of New Rare-Earth Oxborate for Dosimetric Use"

- **Synthesis of new phosphor dysprosium oxoborate($Dy_2B_4O_9$) for thermoluminescence dosimetry application (TLD):**

The initial part of the project is to synthesis of rare earth dysprosium oxoborate phosphor. To complete the fulfillment of project different oxoborate phosphors doped with various rare earth ion with different concentration. The combustion synthesis method and solid state reaction method are used to synthesis phosphors. In which the phosphor prepared by combustion synthesis method showed prominent TLD characteristics.

- **Characterizations of rare earth doped dysprosium oxoborate phosphor:**

In the next step, the synthesized phosphor samples has been characterized for the analysis of its structural formation.The lattice parameters of $Dy_2B_4O_9$ were calculated form the x-ray diffraction pattern recorded for the various samples. The host $Dy_2B_4O_9$ consist of lattice parameters a = 5.171Å, b = 5.422Å, c= 6.983 Å, α=101.35, β= 95.13, and γ=103.34, which are calculated using powderXsoftware of x-ray diffraction data analysis. The x-ray diffraction analysis reveals that that $Dy_2B_4O_9$ phosphor have triclinic crystal structure with space group p1. The x=ray diffraction patterns indicate that the crystal structure of doped sample does not change significantly after varying doping concentration. The crystallite size of the samples were calculated from Scherer's formula and Williamson–Hall plot method which is of the order of 20-50 nm. The Fourier Transform Infra-Red spectroscopy results are also consistent with x-ray diffraction result which is prominently outcome of synthesized phosphor.

- **Beta irradiation effect on rare earth doped dysprosium oxoborate phosphor and its thermoluminescence dosimetry behaviour:**

Thermoluminescence (TL) glow curves of RE^{3+} doped$Dy_2B_4O_9$ phosphor were carried out after beta-irradiation by Sr^{90} source. Ce^{3+} doped $Dy_2B_4O_9$ phosphor showed significant TL output after beta-irradiation. The maximum TL intensity of about 20000 units, which is a good TL outcome. TL glow curve intensity of Ce^{3+} doped $Dy_2B_4O_9$ phosphors increases

linearly with doping concentration and exposure dose. The fading of the TL intensity is very low for the storage of 30 day, which is less than 7%. The reusability of the phosphor were studied for ten cycles, which is consistent for each use for exposure. All the phosphors are very sensitive to the lower doses. The TL parameters obtained for different Ce^{3+} doped $Dy_2B_4O_9$ phosphors are very consistent and nearby the traditional TLDs. The results suggests that the Ce^{3+} doped phosphors may be the potential for environmental dosimetry and accidental dosimetry applications. Other rare earth doped $Dy_2B_4O_9$ phosphors are also examined to investigate thermoluminescence dosimetry in laboratory environment and the results are prominent.

Whether objectives were achieved? : YES

- **Rare-earth doped oxoborate i.e. $Dy_2B_4O_9$ has been prepared with combustion synthesis method and the effect of beta irradiations has been studied.**

All synthesized rare-earth oxoborate samples were firstly irradiated with irradiated by Sr^{90} beta-source having decay rate 5 mCi for different time intervals for the doses of 0.048 to 0.48 Gy with accuracy of ±10%. The irradiation of beta particle induces the defect levels called electron trap and hole trap which store the information about the absorbed radiation. The TL study has been carried out to complete investigate of identification of amount of dose absorbed, time of exposure, energy absorbed to reveal the dosimetry applications of synthesized dysprosium oxoborate ($Dy_2B_4O_9$) phosphors.

- **Effect of thermal treatment on formation of various defects shows the sample can be used for dosimetric purpose.**

To achieve the purpose of TLD application of the dysprosium oxoborate ($Dy_2B_4O_9$) phosphors, TL characteristics of phosphor has been investigated to study the fading effect after exposure, linearity of TL output with doses, sensitivity for the reusability of phosphor were examined through the proper layout of experiments. The prepared phosphors have a low fading effect of TL information, high linearity as after the amount of dose increment, sensitive for small doses and large number of reusing applicability that is the important criterion of TLD phosphor.

- **Calculation of activation energy indicates the confirmation of trap depth in prepared sample.**

The main objective of the project is to study thermoluminescence dosimetry behaviour of the dysprosium oxoborate ($Dy_2B_4O_9$). For that the important parameter such as activation energy and frequency factor has been determined from an experimental TL glow-curve. Various informative TL parameters can be found using these data which is very useful to understand the mechanism associated with the charge transfer process takes place in the material under study. The TL parameters has been calculated through various TL analysis method; Initial rise (IR) method, peak shape methods (PSM), Kitis et al. equation for curve fitting (GCD fitting), and whole glow curve-peak method.

- **The mechanism of thermoluminescence has been explained and photoluminescence sensitivity understood for the sample.**

The occurrence of thermoluminescence form the phosphor is that the electron detraping fromthe electron trap. When the ionizing radiation incident on phosphor, it can excite the electrons from the valence band of the host which can trapped at metastable energy states or in electron trap centers or localized levels. For project objective fulfilment dysprosium oxoborate ($Dy_2B_4O_9$) has been irradiated by beta-radiation and other some clinical x-ray radiation. That induces the electron trapped, when the heat energy is supplied to the phosphor this trapped electrons gets free from the trap and recombine with holes in valance band through the conduction band. The TL emission information is recorded in the form of TL glow curve, which contains the whole information about the absorbed radiation. The photoluminescence emission of the phosphor has been recorded to investigate the optical properties of the dysprosium oxoborate ($Dy_2B_4O_9$). The creation of localized energy levels or luminescent centres in energy gap can be induce due to defect or incorporation of intentionally doped impurity within the crystal lattice of host in the form of substitutional or interstitial positions, or cation and anion vacancies which are responsible for the high yield photoluminescence and thermoluminescence.

- **It is achieved that the rare doped oxoborate is found suitable for the beta radiation dosimetry.**

The TLD application of the dysprosium oxoborate ($Dy_2B_4O_9$) has been identified by creating the clinical environment in laboratory frame, where the dysprosium oxoborate ($Dy_2B_4O_9$) samples were irradiated for lower dose of beta radiation for 0.048 to 0.48 Gy with accuracy of ±10%. The identically require criterion for good TLD and clinical dosimetry has been successfully investigatedthat revealed the phosphor is prominent for dosimetry.

Research article in National Journals:

1. Photoluminescence studies of doped and undoped Dysprosium Oxoborate Verma Vishwnath, **M. Srinivas**, Niemsh Patel, Dhaval Modi, K. V. R. Murthy, Proceedings of the National Seminar on Display Materials ISBN (Offline): 987-93-82570-42-4, Page no. 44-47.

Paper presentations in National seminars/conference:

1. Synthesis and characterization of doped and undoped Dysprosium Oxoborate

   M. Srinivas, Verma Vishwnath, Nimesh Patel, and K.V.R. Murthy

   National Conference on Luminescence and Its Applications (NCLA-2014), 5-7th February, 2014, Jabalpur, India.